

1 **Seasonal variability, sources, and parameterization of ice-nucleating particles in the**
2 **Rocky Mountain region: Importance of soil dust and biological contributions**

3

4 **Ruichen Zhou, Russell Perkins, Drew Juergensen, Kevin Barry, Kelton Ayars, Oren Dutton,**
5 **Paul DeMott, Sonia Kreidenweis**

6 Department of Atmospheric Science, Colorado State University, Fort Collins, Colorado 80523,
7 USA

8

9 Corresponding author: Russell Perkins (rperkins@colostate.edu)

10

11

12

13

14

15 **Abstract**

16 Atmospheric ice-nucleating particles (INPs) significantly influence cloud microphysics and
17 aerosol-cloud interactions. ~~Given that mountainous regions are vital to water resources,~~
18 ~~understanding~~ Understanding of INPs in ~~these areas~~ mountain regions is important for predicting
19 impacts on regional clouds and precipitation. In this study, we conducted comprehensive
20 measurements of immersion-freezing INPs at Mt. Crested Butte in the Rocky Mountains from
21 September 2021 to June 2023 as part of the Surface Atmosphere Integrated Field Laboratory (SAIL)
22 campaign. The average number concentration of INPs active at -20°C was 2 L^{-1} , with distinct
23 seasonal variation characterized by high summer concentrations and low winter concentrations.
24 Aerosol sources were resolved, and INP concentrations were correlated with a coarse dust aerosol
25 type, which dominates PM_{10} in this region. Calculating Converting INP concentrations to IN active
26 surface site densities (n_s) ~~led to reduction in variability~~, further supporting ~~a relationship~~
27 ~~between~~ the primary contribution from coarse dust ~~and to~~ INPs. ~~Reduction of INP concentrations~~
28 ~~following~~ tTreatment with H_2O_2 ~~indicated~~ indicated substantial contributions (91% on average)
29 from organic INPs across all activation temperatures, suggesting that supermicron organic-
30 containing soil dust dominates the INPs in this region. Heat-labile INPs, likely biological in origin,
31 were identified as dominant at $> -15^{\circ}\text{C}$ through heat treatment of samples and showed
32 significantly lower contributions in winter (~96% reduction). Parameterizations based on n_s for
33 the INPs observed in this mountainous region were developed, which effectively reproduced
34 measured INPs concentrations, particularly when accounting for seasonal differences. This study
35 provides the first long-term, comprehensive characterization of INPs for the Upper Colorado River
36 Basin region and offers a parameterization potentially useful for predicting INPs in other remote
37 continental regions.

38 **1. Introduction**

39 Atmospheric aerosols play critical roles in forming clouds, and inadequate understanding of
40 aerosol-cloud interactions presents one of the largest uncertainties in predicting global climate
41 (IPCC, 2022; Seinfeld et al., 2016). The subset of aerosol particles that serves as ice-nucleating
42 particles (INPs) can trigger heterogeneous freezing of cloud water droplets, allowing them to
43 freeze above the homogeneous freezing temperature (approximately -38°C) (Hoose and Möhler,
44 2012). Among the mechanisms of heterogeneous freezing, this immersion freezing process is
45 considered the most important process for mixed-phase clouds, which are common at midlatitudes
46 in all seasons (Kanji et al., 2017; De Boer et al., 2011). These INPs are responsible for a significant
47 proportion of initial cloud ice phase formation, thus impacting the Earth's radiative balance and
48 precipitation (Lohmann and Feichter, 2005; Kanji et al., 2017; Burrows et al., 2022). Although
49 INPs are increasingly a focus of study, the sources and abundances of INPs are not well
50 characterized for many regions.

51 Various aerosol sources have been found to contribute to INPs, including natural and
52 anthropogenic sources (Kanji et al., 2017). Atmospheric mineral dust particles are considered a
53 dominant contributor of INPs throughout much of the troposphere, ~~especially at colder~~
54 ~~temperatures~~ (Murray et al., 2012; Hoose and Möhler, 2012). ~~Mineral dust and they presents~~
55 ~~efficient ice nucleating ability produce high INP concentrations in a mass or surface area basis~~ at
56 temperatures lower than -15°C (Atkinson et al., 2013; Kiselev et al., 2017). Mineral INPs are
57 inorganic components that are lofted from rock or soil and can undergo long range transport to
58 remote areas (Knippertz and Stuut, 2014). In contrast, soil dusts from agricultural or grazed fields
59 (arable soils) were suggested to contribute 25% of the global dust burden (Ginoux et al., 2012),
60 and were found to initiate ice nucleation at temperatures as high as -6°C (Garcia et al., 2012;

61 O'Sullivan et al., 2014). Organics in arable soil dust are suggested as the main contributors to their
62 ice nucleating ability (Tobo et al., 2014; Hill et al., 2016). Biomass burning aerosols and fly ash
63 also contribute to INP populations and have received increasing attention under global warming
64 and the accompanying more frequent and intense wildfires (Prenni et al., 2012; ~~Meeluskey~~
65 McCluskey et al., 2014; Umo et al., 2015). Biomass burning aerosols typically present lower ice
66 nucleating ability, defined as the IN active surface site density for ice nucleation on particle
67 surfaces (i.e., INP concentration/aerosol surface area concentration), compared to dust particles,
68 while atmospheric aging can potentially enhance their ice nucleating ability (Jahl et al., 2021).
69 Biogenic aerosols, such as primary biological particles composed of bacteria, pollen, fungal spores,
70 and their fragments, were identified in the 1970s as important INP sources (Vali and Schnell, 2024;
71 Schnell and Vali, 2024). They typically can activate ice formation at a warmer temperature than
72 other INPs listed above and thus may control first ice formation in clouds (Pratt et al., 2009;
73 Creamean et al., 2013; Tobo et al., 2013). Besides these INP sources, marine aerosol (Wilson et
74 al., 2015; ~~Meeluskey~~McCluskey et al., 2018b), secondary organic aerosol, and fuel-combustion
75 aerosols can contribute to INPs (Kanji et al., 2017).

76 To estimate INPs for use in numerical cloud models, early parameterizations were typically based
77 on empirical relationships between INPs and temperature or supersaturation alone (Bigg, 1953;
78 Meyers et al., 1992). These parameterizations could show large biases compared to field
79 observations. DeMott et al. (2010) proposed a widely used parameterization based on temperature
80 and number concentrations of particles larger than $0.5 \mu\text{m}$ in diameter, which has been applied in
81 global and regional models due to its convenience and independence from detailed aerosol
82 composition (Miltenberger et al., 2018; Storelvmo et al., 2011; Burrows et al., 2022). However,
83 recent studies highlight the need for more physically based and source-specific parameterizations

84 (Burrows et al., 2022; Shi and Liu, 2019; DeMott et al., 2015). Laboratory and field studies have
85 shown that different aerosol types (e.g., mineral dust, biological particles, marine aerosols) exhibit
86 distinct ice-nucleating efficiencies (Hoose and Möhler, 2012; Kanji et al., 2017). Parameterizations
87 based on the ice-nucleating IN active surface site density ($n_s(T)$) have been developed for various
88 aerosol types under immersion freezing conditions (Niemand et al., 2012; DeMott et al., 2015;
89 Harrison et al., 2019; ~~Meeluskey McCluskey~~ et al., 2018a; Umo et al., 2015; Schill et al., 2020;
90 Tobo et al., 2014; O'Sullivan et al., 2014). Further field observations and laboratory studies are
91 needed to improve these parameterizations and reduce uncertainties in INP predictions.

92 Mountainous regions, covering approximately one-quarter of the global land surface, play a critical
93 role in regional and global hydrological and climatic systems. Importantly, they are sources of
94 freshwater supporting nearly half of the world's population (Viviroli et al., 2007). Cloud and
95 precipitation formation in mountainous areas are strongly influenced by aerosol–cloud interactions
96 (Lynn et al., 2007). The presence, variability, and sources of INPs in mountain areas can
97 significantly affect cloud phase, lifetime, and precipitation efficiency (Creamean et al., 2013; Lynn
98 et al., 2007). However, INP observations in mountain environments, especially for long-term
99 continuous measurements, are limited (Lacher et al., 2018; Sun et al., 2024; Conen et al., 2015),
100 hampering our understanding of INP major sources, seasonal variation, and the influence of
101 complex mountain terrain on their vertical distribution. Improved understanding of INPs in
102 mountainous regions is essential for better representation of clouds and precipitation formation in
103 weather and climate models, and for predicting future changes in water availability under global
104 climate change regimes.

105 The Surface Atmosphere Integrated Field Laboratory (SAIL) Campaign, conducted from
106 September 2021 to June 2023 in the Upper Colorado River Basin of the Rocky Mountains,

107 included aims to improve understanding of how aerosols, particularly long-range transported dust
108 and wildfire smoke, affect the surface energy and water balance through their impacts on cloud,
109 precipitation, and surface albedo, and how these effects vary by season (Feldman et al., 2023).
110 This campaign provided a unique opportunity to investigate INPs in the Colorado Rocky
111 Mountains over a nearly two-year period. This study presents comprehensive measurements of
112 immersion-freezing INPs, including their seasonal and temperature-dependent variability, as well
113 as associations with aerosol sources. We further explore different INP compositional types,
114 biological/heat-labile, other organic, and inorganic INPs, and their inter-relationships, highlighting
115 the importance of organic INPs. A parametrization method is proposed for INPs in this region that
116 reproduces the observed two-year INP concentration record.

117

118 **2. Methods**

119 **2.1 Sampling site and sample collection**

120 The SAIL campaign deployed the Department of Energy Atmospheric Radiation Measurement
121 (DOE ARM) Mobile Facility 2 (AMF-2) at the East River Watershed, which is located near Crested
122 Butte and Gothic, Colorado (Feldman et al., 2023). This mountainous region, with elevations
123 ranging from ~2440 to 4350 m above sea level, is characterized by complex terrain, a deep seasonal
124 snowpack, and pronounced hydrometeorological gradients. The region experiences strong
125 seasonal contrasts, with cold snowy winter and warm summers influenced by convective activity
126 associated with the North American monsoon (Feldman et al., 2023).

127 For INP analyses, aerosol filter samples were collected by DOE ARM technicians through the INP
128 Mentor Program approximately every three days from September 2021 to June 2023, with each

129 sampling period lasting about 24 hours, as described in the instrument handbook (Creamean et al.,
130 2024) and repeated briefly here. Aerosols were collected on two 47 mm Nuclepore polycarbonate
131 filters (0.2 μ m pore size) at flow rates in the range of 10–18 lpm, with total sampling volumes of
132 approximately 15000 to 25000 L. For computing atmospheric concentrations in this study, the
133 sampling volume was corrected to standard temperature (273.15 K) and pressure (101.3 kPa). Prior
134 to sampling, the filters were cleaned using 10% H_2O_2 and deionized (DI) water to remove organic
135 and biological residues, then stored in sterile Petri dishes. For the first month (September 2021) of
136 the campaign, samples were collected at the M1 site (38°57'22.35"N, 106°59'16.66"W at 2885 m
137 MSL). From October 2021 to June 2023, samples were collected at the S2 site (38°53'52.66"N,
138 106°56'35.21"W at 3137 m MSL). The distance between M1 and S2 sites is about 8 km. The
139 possible difference in INP concentrations at M1 in the first month is not addressed here, since this
140 study is aimed at representing the INPs in this region, and there was no significant change in INP
141 concentrations when moving from the M1 to the S2 site. All samples were stored at -20 °C after
142 collection, during shipment, and until the analysis in the laboratory.

143

144 **2.2 Laboratory Ice Spectrometer analysis of filter-collected particles**

145 The immersion freezing ability of particles collected on filters was quantified using the Colorado
146 State University (CSU) Ice Nucleation Spectrometer (INS), following established procedures
147 ([Meeluskey McCluskey](#) et al., 2017; Hiranuma et al., 2015; Barry et al., 2021a), which are the
148 same methods used by the DOE ARM INP Mentor Program (Creamean et al., 2024). The INP
149 Mentor Program analyzed many of the samples from the SAIL campaign. Our analysis was used
150 to fill gaps in time for the Mentor Program samples, and provide additional heat and hydrogen
151 peroxide treatments, described below. Our data on these samples is provided within the Mentor

152 Program data product (Shi et al., 2025). Briefly, exposed filters were mixed with 10 mL of filtered
153 deionized water in a centrifuge tube, then rotated for 20 minutes using an end-over-end shaker to
154 resuspend the particles. Aliquots of the resuspension solution were pipetted into a 96-well PCR
155 tray and cooled at a rate of 0.33 °C min⁻¹ from room temperature to -30 °C in the CSU INS. The
156 number of frozen wells was recorded at 0.5 °C intervals, ~~and~~ Cumulative and INP concentrations ~~were~~
157 ~~calculated~~ as a function of temperature ($n_{INPs}(T)$, INPs per liter of air) were calculated using ~~based~~
158 ~~on~~ the method of (Vali, (1971) ~~using~~:

$$159 \quad n_{INPs}(T) = \ln\left(\frac{N_0}{N_0 - N(T)}\right) \times \frac{V_w}{V_c} \times \frac{1}{V_a}$$

160 where N_0 is the total number of wells containing aliquots, $N(T)$ is the cumulative number of wells
161 frozen at temperature T , V_w is the volume of water used for particle resuspension, V_c is the aliquot
162 volume added to each well, and V_a is the total sampled air volume. Counting uncertainties were
163 estimated using binomial confidence intervals (Agresti and Coull, 1998). Field blank filters were
164 collected every month by briefly exposing them at the sampling site for several seconds before
165 ~~removal and~~ storage. Before calculating INP concentrations, the average number of INPs versus
166 temperature per blank filters was subtracted from the calculated number of INPs versus
167 temperature per sample filter, to account for potential contamination during sampling and handling,
168 as well as any residual contamination on the filters after cleaning.

169 To further characterize the types of INPs, portions of the suspended aerosol solution were subjected
170 to heat and hydrogen peroxide (H₂O₂) treatments, followed by freezing analysis of aliquots of these
171 portions. For heat treatment, the solution was heated to 95 °C for 21 min before measurement. This
172 process inactivates the biological INPs by denaturation of proteins and removes heat-labile INPs
173 (O'Sullivan et al., 2014; Tobo et al., 2014; Hill et al., 2016). In total, 43 samples were exposed to

174 95 °C heat treatment, and their temperature spectra are shown in Figure S1. In the peroxide
175 treatment, 30% H₂O₂ was added to the solution to make a final concentration of 10%, and the
176 mixture was heated at 95 °C for 21 min under UVB light to digest organics (Suski et al., 2018),
177 and the INPs remaining were presumed to be inorganic. A total of 34 samples underwent H₂O₂
178 treatment, with their temperature spectra shown in Figure S2. By comparing untreated (base), heat-
179 treated, and H₂O₂-treated results, INPs were categorized into biological/heat-labile, other organic,
180 and inorganic types. Daily et al. (2022) found that some minerals also showed reduced immersion-
181 freezing activity after heat treatment; however, SAIL samples showed some difference with the
182 behaviors they reported. For minerals with initial active temperatures > -10 °C, IN active surface
183 site density either decreased at all measured temperatures (Arizona Test Dust (ATD) and Fluka
184 Quartz) or was not sensitive to wet heating (K-feldspar) (Daily et al., 2022), differing from some
185 spectra of SAIL samples that only showed decreases at warm temperatures and almost no change
186 at temperatures < -18 °C (Figure S1). This suggests that mineral INPs have limited contributions
187 to the decreases of INP concentrations after heat treatment in the SAIL samples.

188 There were eight ground-based sites within 55 km of the SAIL sampling locations conducted
189 orographic cloud seeding operations by North American Weather Consultants Inc., targeting
190 precipitation enhancement. To the best of our knowledge, these seeding stations combusted
191 solutions in a propane flame, producing particles containing silver iodide (AgI) and other inorganic
192 salts that served as seeding aerosols. These seeding activities occurred in specific storm situations
193 during winter and early spring and strongly impacted our INP observations. The measured
194 concentrations of INPs active at temperatures from -7.5 °C to -27.5 °C for a total of 113 24-hour
195 samples are shown in Figure S3. Since this work focuses on investigating the natural or background
196 INPs in the Rocky Mountain region, samples collected on days that overlapped with artificial cloud

197 seeding activities, as recorded in their logbook (data provided by North American Weather
198 Consultants Inc.), are highlighted in Figure S3 and excluded from the discussion below. Cloud
199 seeding activities last less than 24 hours, typically 4-8 hours, and are unlikely to affect the
200 subsequent sample collected 3 days later. Also, eight samples collected during winter exhibited
201 distinct INPs spectra from other samples, but highly similar to the INP spectrum of Snomax®, a
202 commercial non-living bacterial INP product used in snowmaking (Figure S4a). Furthermore, *P.*
203 *syringae*, the bacterium type in Snomax, was identified in some of these samples based on qPCR
204 analysis (Supplement Text S2, Figure S4b). These samples are highly suspected to have been
205 affected by snowmaking activities during wintertime, associated with the location of sampling site
206 within a ski resort at Crested Butte. Therefore, these samples, along with those affected by cloud
207 seeding activities, were excluded from the subsequent discussion to better understand the
208 characteristics of natural INPs in the Rocky Mountain region.

209

210 **2.3 Source apportionment**

211 To investigate aerosol sources in the SAIL region, source apportionment was performed using
212 positive matrix factorization (PMF). PMF is a receptor model that decomposes an observation
213 matrix into factor profiles and their corresponding contributions related to emission sources and/or
214 atmospheric processes, providing a quantitative assessment of source influences (Paatero and
215 Tapper, 1994). Data from the Interagency Monitoring of Protected Visual Environments
216 (IMPROVE) site at White River, located approximately 30 km north of the SAIL campaign site,
217 were used for PMF analysis. The IMPROVE network (Malm et al., 1994) has collected 24-hour
218 aerosol filter samples every three days over several decades at this site, providing a valuable dataset
219 to understand aerosol sources and their long-term variability in the region. In the IMPROVE

220 program, elemental analysis was performed on the Teflon filters using X-ray fluorescence (XRF),
221 anions were analyzed using ion chromatography (IC), elemental carbon (EC) and organic carbon
222 (OC) were analyzed using a carbon analyzer (Hand, 2023). Chemical concentrations in the PM_{2.5}
223 fraction of nineteen elements (Al, As, Br, Ca, Cl, Cr, Cu, Fe, K, Mg, Mn, Na, Ni, Pb, Se, Si, Ti, V,
224 and Zn), along with nitrate, sulfate, elemental carbon (EC), organic carbon (OC), and calculated
225 coarse mass concentrations (PM₁₀–PM_{2.5} mass concentrations), from January 2014 to April 2024
226 were used as input for the PMF analysis performed using EPA PMF 5.0 (Norris et al., 2014).
227 IMPROVE species concentrations were reported based on local conditions.

228 A five-factor solution was selected as the optimal solution based on the Q/Q_{exp} value and
229 interpretation of the physical meanings of the factors (Brown et al., 2015). The corresponding
230 factor profiles and time series are shown in Figures S5 and S6. These factors were identified, based
231 on chemical signatures and previous literature, as coarse dust, fine dust, biomass burning, sulfate-
232 dominated, and nitrate-dominated sources. Coarse and fine dusts had high contributions from Al,
233 Ca, Fe, Mg, and Si, which are the main components of mineral dust (Liu and Hopke, 2003). Coarse
234 dust explained more than 90% of the coarse mass (> PM_{2.5}), while there was no contribution from
235 coarse mass in the fine dust factor. The biomass burning factor was strongly associated with
236 organic and elemental carbon, which are mainly from combustion processes, and K, a tracer of
237 biomass burning (Hopke et al., 2020). The other two factors are dominated by nitrate and sulfate,
238 which are related to the formation of secondary aerosols and possibly some primary emissions
239 from regional sources that include energy production and distant urban regions. Some similar
240 factors were also resolved in published PMF analyses using IMPROVE data (Liu and Hopke, 2003;
241 Hwang and Hopke, 2007). Further details on the PMF analysis and results, as well as support for
242 their applicability over the broad surrounding Rocky Mountain region (IMPROVE sites at Mount

243 [Zirkel and Rocky Mountain National Park](#)) are provided in Supplement Text S1 and Figure S7.

244 Data for the PMF results are available through the ARM data product (Zhou et al., 2025a).

245 To assess the impact of different sources on INPs, the INP samples were categorized into six types

246 based on the dominant aerosol sources during the sampling period, [and the contribution of sources](#)

247 [to each sample was shown in Figure S8](#). However, IMPROVE samples were taken only one of

248 every three days. For days without available IMPROVE data, aerosol sources were inferred from

249 the nearest sampling days. Samples were classified as follows: (1) [Coarse dust, if coarse dust](#)

250 [contributed more than 50% to the total PM₁₀ mass concentration or contributed more than 40%](#)

251 [and represented the largest contribution among all sources](#) ~~Coarse dust, if coarse dust contributed~~

252 ~~more than 40% to the total PM₁₀ mass concentration~~; (2) Biomass burning, if biomass burning

253 accounted for more than 50% of the total PM₁₀; (3) Dust, if the combined contribution of coarse

254 and fine dust exceeded 50% of the total PM₁₀, with the difference between fine and coarse dust

255 being less than 20%; (4) Fine dust, if the combined mass contribution of coarse and fine dust

256 exceeded 50% of the PM₁₀ and fine dust exceeded coarse dust by more than 20%; (5) Mixed

257 samples, samples for which no single source was dominant, typically characterized by a sulfate

258 contribution greater than 20% of the PM₁₀. (6) Additionally, seven samples fell within periods

259 where more than one consecutive IMPROVE sample was missing (one week or longer). For these

260 cases, source contributions were not interpolated, and they were categorized as samples with no

261 source data. Source influences inferred from the nearest sampling days may introduce uncertainties.

262 However, the merged size distribution data (section 2.5 and Figure 2) for these days showed similar

263 size distribution patterns and comparable number concentrations for most size ranges compared to

264 the nearest days, suggesting that significant changes in aerosol sources for these inferred days were

265 limited. Also, the discussion is based on each group containing multiple samples, which should
266 also reduce the uncertainties associated with the inferred source from a single sample.

267

268 **2.4 Back trajectory analysis**

269 Air mass back trajectory analysis was performed using the Hybrid Single-Particle Lagrangian
270 Integrated Trajectory model (HYSPLIT; Stein et al., 2015; Rolph et al., 2017), developed by the
271 National Oceanic and Atmospheric Administration (NOAA) Air Resources Laboratory. For each
272 hour during each sampling period (typically 24 h), a 96-hour back trajectory was initiated at the
273 SAIL sampling site, starting 100 m above ground level, and using the GDAS meteorological
274 dataset with model vertical velocity. The areas traversed by the back trajectory were gridded into
275 $1^\circ \times 1^\circ$ cells. For each trajectory, its occurrence in each grid cell was weighted by the residence
276 time spent in that cell. To account for the peak in occurrence near the sampling site, the residence
277 times were further normalized by the distance from the SAIL sampling site, following the method
278 of [Ashbaugh et al., \(1985\)](#). The analysis was performed for each sample, and the resulting
279 trajectories were aggregated to produce a composite residence-time map (Figure 1). Separate
280 analyses were also performed for samples categorized by different source types (Figure [S8S9](#)),
281 aggregating hourly trajectories for all sample times of a corresponding type across the campaign.
282 Back trajectory data are available through the ARM data product (Zhou et al., 2025b).

283

284 **2.5 Merged particle number-size distribution and IN active surface site density**

285 During the SAIL campaign, a scanning-mobility particle sizer (SMPS) and an optical particle
286 counter (OPC) were deployed simultaneously with the filter sample collection to measure aerosol

287 number size distributions in the particle diameter ranges from 10–500 nm and 0.25–35 μm ,
288 respectively (Kuang et al., 2024; Cromwell et al., 2024). To obtain a continuous number size
289 distribution from 10 nm to tens of micrometers, measured number size distributions from the
290 SMPS and OPC were merged following previous methods (Hand and Kreidenweis, 2002;
291 Marinescu et al., 2019). Briefly, the mobility diameters from the SMPS were assumed to be equal
292 to volume equivalent diameters by assuming the particles are spherical, and number distributions
293 were converted to volume distributions. A scaling factor was determined by comparing the
294 overlapping size range of the two instruments, and the OPC volume size distribution was then
295 aligned with the SMPS volume distribution measurements by shifting OPC measured diameters to
296 estimate the SMPS mobility diameter corresponding to that optical diameter. All aerosol data from
297 the ARM archive were corrected to standard temperature (273.15 K) and pressure (101.3 kPa). All
298 merged size distribution data are available through the ARM data product (Zhou et al., 2025c). A
299 timeline of the merged number-size distributions of aerosols during the SAIL campaign is shown
300 in Figure 2.

301 Assuming that the number of active ice ~~-nucleat~~ioning sites is linearly proportional to the particle
302 surface area, the IN active surface site density (m^{-2}) at temperature T ($n_s(T)$, m^{-2}) was calculated
303 using the following equation:

$$304 \quad n_{s,500}(T) = \frac{n_{\text{INP}}(T)}{S_{\text{m},500}} \times 10^9$$

305 where $n_{\text{INP}}(T)$ (sL^{-1}) is the measured INP concentration at temperature T , $S_{\text{m},500}$ ($\mu\text{m}^2/\text{scm}^3$) is the
306 surface area concentration of particles larger than 500 nm diameter calculated from the merged
307 size distribution, assuming that particles are spherical, and the 10^9 conversion factor is used for
308 $n_{s,500}$ units of m^{-2} . In this study, the surface area of particles > 500 nm is used to exclude surface

309 area associated with pollution and other aerosol types that are inefficient sources of INPs. This is
310 supported by the correlation found between INP concentrations and the number concentrations of
311 particles > 500 nm in a previous study (DeMott et al., 2010). The n_s is also calculated based on
312 total surface area concentrations to facilitate comparison with other studies and is shown in Figure
313 S105. While the IN active surface site density approach is typically fully justified for single INP
314 compositions, we will apply it here to the total surface areas, but also discuss adjustments needed
315 when comparing to more specific INP parameterizations.

316

317 **3. Results and Discussion**

318 **3.1. INPs concentrations at the SAIL study site**

319 Samples not affected by artificial INP generation activities (cloud seeding and snowmaking
320 activities in winter; see section 2.2), representing the natural INPs in this region (84 samples in
321 total), are shown in Figure 3a. The discussion in this study focuses on these samples to better
322 understand the characteristics of natural INPs in the Rocky Mountain region. INP concentrations
323 ranged from 4×10^{-4} L $^{-1}$ to 1.5 L $^{-1}$ (mean: 0.15 L $^{-1}$, median: 0.05 L $^{-1}$) at -15 °C, and from 1.2
324 L $^{-1}$ to 90 L $^{-1}$ (mean: 16 L $^{-1}$, median: 12 L $^{-1}$) at -25 °C. [This is comparable to online INP](#)
325 [measurements in the Rocky Mountain region \(median: 8.2 L \$^{-1}\$ at \$-26\$ °C; Lacher et al., 2025\).](#)

326 Compared with previous INP studies summarized by Kanji et al. (2017), the INP concentrations
327 observed during the SAIL campaign fall within the range of those in their compilation that were
328 influenced by dust, biomass burning, and precipitation, and are higher than those from marine
329 aerosols but lower than the maximum of those attributed to biological sources. Regarding temporal
330 variations, INP concentrations at all measured temperatures followed a similar trend over the

331 nearly two-year observation period: low in winter, increasing in spring, and reaching highest
332 concentrations during summer and early fall. For activation temperatures warmer than $> -25^{\circ}\text{C}$,
333 the highest INP concentrations were all observed in summer. For temperatures colder than $< -25^{\circ}\text{C}$,
334 the samples from summer also showed high INP concentrations, while the peak concentrations
335 occurred in September 2021. Back trajectories of those samples (2021-9-9 and 2021-9-16) showed
336 that the air masses mainly originated from the northwestern U.S. Intense wildfires occurred in that
337 region during the summer of 2021 (Jain et al., 2024). ~~and smoke plumes were and the~~ transported
338 smoke plumes increased aerosol loading at the SAIL site. These smoke intrusions may also,
339 ~~which significantly increased aerosol loading and result in~~ enhanced INPs concentrations active at
340 low temperatures.

341 Monthly mean INP concentrations were calculated and are presented in Figure 3b, to better
342 visualize seasonal trends and reduce the impact of individual outliers. INP concentrations showed
343 clear seasonal variations throughout the campaign. Note that our sampling did not cover the entire
344 month, so some outliers may have been coincidentally captured or missed, however, the two-year
345 monthly dataset is still expected to broadly represent the seasonal variations of INPs in this region.
346 In general, INP concentrations reached peaks in June 2022 across all temperatures, and reached
347 minimum levels during winters in both years. However, differences existed among activation
348 temperatures. At warmer temperatures (-10°C and -15°C), INP concentrations were relatively
349 similar in warm seasons (April–October) and much higher than those in cold seasons (November–
350 March). Bioaerosols are typically recognized as major INP sources at these activation temperatures
351 (Kanji et al., 2017), and their emissions generally decrease in winter in most areas due to reduced
352 biological activities and possible snow cover limiting resuspension (Fröhlich-Nowoisky et al.,
353 2016). A distinct high INP peak was observed in June 2022, which was ten times higher than that

354 in June 2023, and much higher than in other months, suggesting that a high INP emission event
355 occurred during this month, which may be related to a specific biological emission event and/or
356 dust event. For activation temperatures of -20°C and -25°C , INP concentrations also showed a
357 seasonal pattern increasing from April, peaking in June, then decreasing and reaching a minimum
358 in December. [Recent online INP measurements for activation temperatures from \$-22^{\circ}\text{C}\$ to \$-32^{\circ}\text{C}\$](#)
359 [conducted from October 2021 to May 2022 and January to May 2025 at the Storm Peak Laboratory](#)
360 [in the Rocky Mountains \(Lacher et al., 2025\) found a similar seasonal pattern, with the lowest INP](#)
361 [concentrations in winter and increased in spring, suggesting that the INP sources could be similar](#)
362 [and may dominate INPs across a broad region of the Rocky Mountains.](#) The elevated INPs from
363 April to September may be attributed to enhanced dust aerosols, as dust concentrations were found
364 to increase during this period (Hand et al., 2017), [as-and](#) dust is a significant source of INPs,
365 especially at [lower](#) temperatures [below \$-15^{\circ}\text{C}\$](#) (Kanji et al., 2017; DeMott et al., 2015). Lower-
366 temperature INP concentrations in June 2022 were also higher than those in June 2023, while
367 the magnitude of this difference (a factor of two) was less distinct from the difference at -10°C
368 (twelve times). This suggests that the origins of INPs activated at lower temperatures differ from
369 those at warm temperatures.

370

371 **3.2. Relationships between aerosol sources and INPs**

372 The sources of aerosols to the SAIL campaign region were identified based on the PMF analysis
373 (Text S1, Figures S5 and S6). Different sources exhibited unique seasonal trends. Coarse dust
374 showed increased concentrations from April to September and had the highest annual mean
375 concentration among the five resolved particle types. Fine dust increased sharply in April, May,
376 and June, and remained low during other months. Biomass burning aerosol varied significantly by

377 year. Strong peaks in concentrations were observed in September 2021, with SAIL collecting some
378 samples at the end of these events, and increased contributions in June–August 2022. The biomass
379 burning factor typically showed high concentrations in summer. The sulfate-dominated and nitrate-
380 dominated factors had much lower concentrations overall, with peaks occurring in summer and
381 spring, respectively. The aerosol number size distribution also reflected the variations in different
382 sources (Figure 2). Supermicron particle concentrations were higher when coarse dust increased.
383 Submicron particles concentrations increased in September 2021 and the summer of 2022, which
384 corresponded to increases in contributions from the biomass burning factor (Figure 2). To
385 investigate the impact of different aerosol types on INPs, temporal variations between aerosol
386 sources and INP concentrations at -15°C and -25°C were compared, as shown in Figure 4S9.
387 Monthly average concentrations were used to minimize the impact of unsampled dates. Although
388 this may introduce uncertainties by smoothing episodic peaks of a source, the nearly two-year (22
389 months) record should adequately represent its seasonal cycle. Pearson correlation coefficients
390 between monthly INP concentrations (-10°C , -15°C , -20°C , and -25°C) and aerosol sources
391 are shown in Table 1.

392 Coarse dust and biomass burning presented seasonal variations similar to those of INPs at -15°C
393 and -25°C , while fine dust, nitrate-dominated, and sulfate-dominated factors had weaker
394 correlations (Figure 4). The strong correlations with coarse dust and biomass burning aerosols
395 suggest that these sources significantly contributed to observed INPs. Coarse dust showed good
396 correlations with INPs active at all temperatures (Table 1), with correlation coefficients
397 increasing as temperature decreased for colder temperatures, suggesting that coarse dust is a major
398 source of INPs, particularly at lower temperatures. This is consistent with previous findings that
399 dust dominates the INPs at temperatures below -20°C (Beall et al., 2022; Testa et al., 2021; Kanji

400 et al., 2017). Furthermore, Lacher et al. (2025) provided direct evidence that INPs active at cold
401 temperatures were significantly contributed by supermicrometer particles, which they attributed to
402 dust, in the Rocky Mountains. Their observation site was located near to the IMPROVE site at
403 Mount Zirkel, where our PMF analyses identified similar sources and trends to those near the SAIL
404 (Text S1), suggesting that INPs in both studies were impacted by coarse dust. Interestingly, coarse
405 dust ~~also presented a weaker correlation~~ with INPs at -10°C ($R^2 = 0.43$), a temperature range
406 usually associated with biological INPs. This may be due to the large number of coarse dust
407 particles, biological INPs carried on dust particles, and/or the inclusion of biological particles in
408 the coarse dust factor, as biological particles are mostly supermicron in size (Després et al., 2012).
409 Biomass burning presented a strong correlation with INP at -25°C and weak correlations at
410 warmer temperatures (-10°C and -15°C), suggesting that aerosols from biomass burning
411 contribute primarily to INPs active at lower temperatures. Combining coarse dust and biomass
412 burning contributions showed an even better correlation with INPs (Table 1), supporting that these
413 are the major contributors of INPs in this region, especially at lower activation temperatures.

414 Different from coarse dust, fine dust showed weak relationships with INPs at all temperatures (R^2
415 = 0.10–0.19), suggesting lower contributions to INPs. One possible reason is that larger particles
416 have more ice nucleation active sites (Reicher et al., 2019; DeMott et al., 2010). Another reason
417 could be differences in sources of fine and coarse dust that resulted in different ice-nucleating
418 abilities. Fine dust presented a different seasonal pattern compared to coarse dust. Fine dust
419 concentrations peaked in spring, especially in April, while coarse dust was higher in summer. This
420 difference was also observed in Hand et al. (2017) for the Colorado Plateau and Central Rockies
421 regions. They suggested that fine dust in this region is influenced by regional or long-range
422 transported dust, such as Asian dust, while coarse aerosol mass concentrations (defined as the

423 difference between PM₁₀ and PM_{2.5}, which was almost all loaded into the coarse dust factor in our
424 PMF analysis) are mainly derived from local and regional sources. Sulfate-dominated and nitrate-
425 dominated sources were not correlated with INP concentrations. In remote areas, sulfate and nitrate
426 particles mainly come from secondary formation (Seinfeld and Pandis, 2016) and are generally
427 not considered as efficient INPs (Kanji et al., 2017).

428

429 **3.3. INP temperature spectra categorized by sources**

430 The total INP temperature spectra categorized by dominant aerosol types are shown in Figure 4a5a,
431 and total INP spectra sorted under dominant influence of each source type are plotted separately
432 in Figure S10S11. Significant differences in INP concentrations were observed between periods
433 where different aerosol source types were dominant. Over 50% of the samples were dominated by
434 coarse dust, which was the predominant aerosol source in this region (Figure S6S8). Considering
435 that coarse dust also showed a strong correlation with INPs, this suggests INP concentrations were
436 mainly likely primarily influenced controlled by coarse dust in this area. Mineral dust (DeMott et
437 al., 2003; Niemand et al., 2012; Atkinson et al., 2013), soil dust that contains abundant organics
438 (Tobo et al., 2014; Steinke et al., 2016; O'Sullivan et al., 2014), and playa dusts (Pratt et al., 2010;
439 Hamzehpour et al., 2022) have been widely investigated, and are considered as important INP
440 sources. Mineral dust and soil dust that contains abundant organics and/or salts have been widely
441 investigated, and are considered as important INP sources (DeMott et al., 2003; Niemand et al.,
442 2012; Atkinson et al., 2013; DeMott et al., 2015; Pratt et al., 2010; Hamzehpour et al., 2022; Tobo
443 et al., 2014; Steinke et al., 2016; O'Sullivan et al., 2014; Testa et al., 2021; Pereira et al., 2022;
444 Kanji et al., 2017). Based on back trajectories for samples categorized as coarse dust-dominated
445 (Figure S8S9), air masses were mostly from local or regional sources (Central Rockies and

446 Colorado Plateau, with additional inputs from the agricultural Imperial Valley in southern
447 California). Considering their larger size and mass, coarse dust particles have relatively short
448 atmospheric transport ranges, and local resuspension of soil is likely a dominant source (Hand et
449 al., 2017). High air mass residence times were also indicated for the Great Salt Lake region,
450 suggesting potential contributions from playa salts. This is consistent with the contributions of Cl
451 and Na in the coarse dust factor profile from the PMF analysis (Figure S5a), and playa salt dusts
452 have also been observed, at least at lower temperatures in the mixed phase regime, to serve as INPs
453 (Pratt et al., 2010; Koehler et al., 2007).

454 Compared to INPs ~~related samples that aerosols dominated by~~ coarse dust, fine dust-~~dominated~~
455 time periods showed lower INP concentrations (Figure 45). Back trajectories also indicated
456 different origin regions from those for coarse dust; samples dominated by fine dust had trajectories
457 mainly from southern California and the Sonoran Desert in Arizona, known as an area with high
458 dust emissions (Ginoux et al., 2012). Fine dust is likely long-range transported as Asian dust (Hand
459 et al., 2017) or from the noted southwestern desert areas. Besides their different origins, the higher
460 INP concentrations associated with coarse dust-~~dominated samples~~ compared to ~~those dominated~~
461 ~~by~~ fine dust can also be attributed to differences in particle size, although confirming this would
462 require data on size-resolved INPs that were not collected. INPs related to biomass burning-~~dominated samples~~
463 ~~presented comparably high concentrations, which could be attributed may be~~
464 ~~related~~ to the significantly elevated aerosol loading during biomass burning events. To assess the
465 ice nucleating activity, with the influence of aerosol concentrations and size distributions
466 accounted for, the IN active surface site density was further investigated.

467

468 **3.4. IN active surface site density (n_s) temperature spectra**

469 The IN active surface site density (n_s) temperature spectra, a measure of INPs per aerosol surface
470 area, are shown in Figure 4b-5b for all samples, categorized by dominant aerosol type. Compared
471 to INP concentrations, the n_s values were less variable at a given temperature, with most samples
472 within one order of magnitude of each other, whereas INP concentrations spanned nearly two
473 orders of magnitude, suggesting that at least some of the variability in INP concentrations can be
474 explained by differences in particle size distributions and concentrations.

475 Samples dominated by a specific aerosol source (coarse dust, dust, fine dust, or biomass burning)
476 exhibited relatively consistent n_s values with some differences among categories. The n_s of samples
477 dominated by coarse dust was similar to or slightly higher than those having both abundant coarse
478 and fine dusts (categorized as dust), suggesting that INPs from coarse dust was the major
479 contributor to INPs in this region have higher IN active surface site density. After normalizing by
480 surface area, the n_s associated with for the fine dust-dominated samples showed closer values with
481 those for of the coarse dust-dominated samples, while still lower than n_s related to coarse dust.
482 This suggests that the lower INP concentrations in the fine dust-dominated samples can be partly
483 attributed to differences in aerosol surface area concentrations, but also to lower active site density
484 due to potentially different INP sources. The differences in n_s related between to coarse dust- and
485 fine dust-dominated samples were limited, likely because there were still small contributions from
486 coarse dust (17% on average), although fine dust dominated these samples (59% on average).

487 During biomass burning events, aerosol number concentrations were significantly enhanced,
488 especially for submicron particles (Figure 2). A correlation was found between the biomass
489 burning factor mass concentrations and the total surface area concentrations of aerosols (Figure
490 S11S12), suggesting that such events significantly increased aerosol surface area concentrations.
491 However, its contributions to INPs could be affected by coarse dust. After normalization by surface

492 area ($S_{m,500}$), the n_s ~~values associated with~~ of INP samples for aerosols dominated by biomass
493 burning were similar to those of coarse dust-dominated samples. ~~However, e~~Compared with
494 previous studies (comparison based on computing n_s using total surface area), these values were
495 higher than n_s -reported from laboratory biomass burning studies (Umo et al., 2015; Jahn et al.,
496 2020) and those reported in ambient biomass burning observations (~~Meeluskey McCluskey~~ et al.,
497 2014; Barry et al., 2021b; Zhao et al., 2024). ~~This is possible because During SAIL, this finding~~
498 may have been due to the presence of coarse dust, which has a much higher n_s than biomass burning,
499 as this aerosol type still contributed moderately to the total aerosols in these samples (an average
500 of 22% of PM_{10}), although biomass burning was the dominant aerosol source (62% on average).
501 Wildfire events could also be a source of airborne dust (Wagner et al., 2018; Meng et al., 2025).
502 From the NOAA Hazard Mapping System (Figure S12S13) and back trajectories (Figure S8S9),
503 these samples were mostly affected by long-range transported biomass burning aerosols
504 originating primarily from wildfires in the northwest and southwest U.S. Aging could enhance the
505 n_s of biomass burning INPs (Jahl et al., 2021) and may also have contributed to higher n_s of these
506 samples.

507 In contrast to the convergence observed in samples dominated by a single source, samples related
508 to mixed sources showed no reduction in variability after normalization by surface area (Figure 4
509 5 and Figure S10S11). Although it is difficult to precisely determine the INP sources for these
510 samples based on current available analyses, this comparison strongly supports the link between
511 INPs and the dominant bulk aerosol sources in this study.

512

513 **3.5 Evidence of biological contribution to INPs**

514 From the INP temperature spectra and n_s for all samples (Figure 45), the spectra for INPs active at
515 temperatures ~~>higher than about~~ -18 °C showed a ~~clear~~ segregation into two groups: one with
516 higher INP concentrations (and n_s) and measured detectable freezing onset temperatures mostly $>$
517 -10 °C, and the other with lower INP concentrations (and n_s) and lower measured detectable
518 freezing onset temperatures, with most of those samples assigned to aerosol sources of mixed and
519 fine dust. We found all samples in the latter group were collected from December to March. At
520 freezing temperatures warmer than ~~-18-15~~ °C, biological INPs are likely to play a more important
521 role (Kanji et al., 2017).

522 Here, we separated samples collected during cold seasons (December–March) and during other
523 seasons (April–November), as shown in Figure 56. This separation clearly shows that on average,
524 INP concentrations were lower in cold seasons, with the most striking difference at temperatures
525 warmer than -15 °C (15% of INPs in other seasons). A further comparison of n_s (Figure 5b6b)
526 showed that samples from cold seasons had similar n_s at temperatures colder than around -18 °C.
527 However, at warmer temperatures, samples from cold seasons showed consistently lower n_s . These
528 results suggest that INPs that activated at temperatures colder than around -18 °C likely originated
529 from similar sources throughout the whole year, which were primarily associated with coarse dust,
530 as discussed above. However, in cold seasons, the contribution from biological INPs was
531 significantly reduced, leading to the divergence in the spectra for temperatures warmer than around
532 -18 °C. This seasonal pattern is supported by the environmental temperature dependence of
533 biological aerosol emissions (Shawon et al., 2025).

534 The likely biological nature of these warmer-temperature INPs was also identified from the heat
535 treatment of samples. A compilation of spectra from all base (untreated) analyses, heat, and H_2O_2
536 treatments is shown in Figure 67. The difference between the base and heat spectra indicated a

537 large contribution (82–94%, 90% on average) of heat-labile INPs at warm temperatures (> -18
538 15 °C), which are presumably biological INPs. Each individual heat spectrum is shown in Figure
539 S1. In September 2021, most samples showed decreased INP concentrations at temperature
540 warmer than -15 °C after heat treatment, while almost no decrease was observed at lower
541 temperatures. This reduction is likely due to denaturing of biological INPs, reducing or removing
542 their IN activity (Hill et al., 2016). Samples from September 2021 were strongly affected by
543 biomass burning (Figure S6). Kobziar et al. (2024) found that biological aerosols can be co-emitted
544 in biomass burning. The presence of biological INPs in smoke plumes was also suggested in
545 aircraft measurements of biomass burning aerosols, which showed base and heat-treated spectra
546 (Barry et al., 2021b) similar to those observed in SAIL samples from September and October 2022.
547 During the SAIL campaign, Shawon et al. (2025) and Ashfiqur et al. (unpublished data) detected
548 biological aerosols using a Wideband Integrated Bioaerosol Sensor (WIBS) and scanning electron
549 microscopy during selected intensive observation periods (June–September 2022 and September
550 2022, respectively), further supporting the presence of biological aerosols during these periods,
551 some of which may be active as INPs. Biological/heat-labile INPs during the cold seasons account
552 for only 4% of those in the other seasons. There were no significant decreases in warm-temperature
553 INP concentrations after heat treatment for samples collected from January to early April 2022 and
554 December 2022 to March 2023, indicating that biological INPs concentrations were very low
555 during the cold seasons. In the other seasons (April–November), many samples showed spectra in
556 which heat treatment significantly decreased INP concentrations at temperatures > -15 °C and
557 almost no change at lower temperatures, suggesting abundant heat-labile INPs, presumably of
558 biological origin.

560 **3.6 Relationships among INPs types inferred from treatments**

561 After H₂O₂ treatment, almost all samples showed significant decreases (83–97%, with an average
562 reduction of 91%)~~1–2 orders of magnitude~~) in INP concentrations across all measured activation
563 temperatures (Figure 6–7 and Figure S2), suggesting substantial contributions from organic INPs
564 through the entire temperature spectrum. The inorganic INPs and other organic INPs were
565 correlated at –15 °C and –25 °C (Figure 78e and 8f), especially at the lower temperature. The
566 correlations clustered around the 10:1 line, with ratios of 14 and 13 at –15 °C and –25 °C,
567 respectively. These results indicated a dominant contribution from organic components suggestive
568 of a soil origin, as previous studies found that soils contain abundant organic INPs in addition to
569 mineral INPs (Tobo et al., 2014; O'Sullivan et al., 2014; Pereira et al., 2022; Suski et al., 2018;
570 Testa et al., 2021). A short-term observational study (DeMott et al., 2025) at the Storm Peak
571 Laboratory in the Colorado Rockies also attributed soil INPs as the dominant INP source in late
572 summer and early fall. These correlations provide further support that the coarse dust factor was
573 mainly from resuspension of local or regional soil dust. Testa et al. (2021) also found a correlation
574 at –25 °C between other organic and inorganic INPs, with a mean ratio of 5.5 in samples from
575 north-central Argentina. Our results and those of Testa et al. (2021) suggest that other organic INPs
576 and inorganic INPs are co-emitted from similar sources. The correlation coefficient increased at
577 lower temperatures, possibly because other organic and inorganic INPs had limited contributions
578 at –15 °C, a range strongly influenced by biological aerosols. Note that INPs from biomass burning
579 could also contribute to this correlation, as they show similar organic and inorganic INP
580 characteristics in their INP spectra (Schill et al., 2020; Barry et al., 2021b). The only exception is
581 sample 2021-10-14, for which similar INP concentrations were observed in the base, heat, and
582 H₂O₂ treatments at temperatures < –15 °C, suggesting that it was likely dominated by mineral dust.

583 Unexpectedly, a correlation was observed between the biological/heat-labile INPs and other
584 organic INPs at -15°C ($R^2 = 0.61$, $n = 29$, Figure 78a). This correlation suggests that increases in
585 heat-labile INPs, presumably biological INPs, were accompanied by increases in organic INPs.
586 This is possibly because both biological and organic INPs during SAIL originated from the same
587 source at this temperature, which was likely soil dust. However, at a warmer temperature
588 (-12.5°C), the correlation was weaker ($R^2 = 0.10$, $n = 20$), possibly because biological INPs from
589 non-soil sources contributed at higher temperatures (Huang et al., 2021), as the ratios between
590 biological/heat-labile INPs and other organic INPs changed from 13 (-15°C) to 43 (-12.5°C). At
591 -25°C , correlations between biological-/heat-labile INPs and other organic INPs were much
592 weaker, and the ratio was much lower (mean ratio of 2).

593

594 **3.7 Prediction of INPs in the Rocky Mountain region**

595 In this study, n_s values were found to be close to those used in the parameterizations derived from
596 studies of agricultural soil (Tobo et al., 2014), desert dust (Niemand et al., 2012), and fertile soil
597 (O'Sullivan et al., 2014) (Figure S13aS14a). Applying the parameterization from Tobo et al. (2014)
598 using the surface area of particles > 500 nm reasonably estimated INP concentrations (Figure
599 S13bS14b), but tended to underestimate them. This is possibly because the equation provided by
600 Tobo et al. (2014) requires an estimation of the surface area of soil particles, which introduces
601 uncertainties when using $S_{m,500}$; accurately estimating surface area of only soil particles in
602 atmospheric samples requires additional analysis. Also, the equation from Tobo et al. (2014) is not
603 valid for $T > -18^{\circ}\text{C}$. The parameterization from O'Sullivan et al. (2014) includes a wider
604 temperature range, while it tended to underestimate in temperatures warmer than -20°C and
605 overestimate at colder temperatures (Figure S13bS14b). The parameterization from Niemand et al.

606 (2012) was derived from desert dust, consisting mainly of mineral dust. Some of their dust samples
607 might have contained arable dust or biological INPs (Beall et al., 2022). Application of their
608 parameterization to our data showed a bias at warm temperatures (Figure [S13b](#)[S14b](#)). Therefore,
609 we developed a parameterization based on the SAIL samples, which could be useful for estimating
610 atmospheric INPs dominated by organic-containing soil dust.

611 Parameterization was based on an assumed relationship between IN active surface site density (n_s ,
612 m^{-2}) calculated from surface area concentrations of particles > 500 nm ($S_{m,500}$) and temperature
613 (T , $^{\circ}C$) over all seasons. First, a single polynomial equation fitted to data from all samples was
614 obtained (Figure [S14S15](#)), and the INP concentrations predicted from this equation and the
615 measured $S_{m,500}$ were compared with the measured INP concentrations (Figure [S14S15](#)). The
616 predicted INPs were mostly within one order of magnitude of the measured values, suggesting this
617 fit generally provides a reasonable estimation of INPs. However, the predicted INPs showed an
618 overestimation trend for some samples around -15 $^{\circ}C$. This is due to the limited contribution of
619 biological/heat-labile INPs in cold seasons.

620 To better represent the INP temperature spectra accounting for the seasonality of biological
621 contributions, parameterization equations were fitted as polynomials for samples from other
622 seasons (April–November, equation 1) and cold seasons (December–March, equation 2) separately
623 (Figure [89](#)), as follows,

$$\ln (n_s) = -0.007T^2 - 0.785T + 6.636 \quad (-30 \text{ } ^{\circ}C < T < -6 \text{ } ^{\circ}C) \quad (1)$$

$$\ln (n_s) = -0.030T^2 - 1.833T - 5.076 \quad (-20 \text{ } ^{\circ}C < T < -10 \text{ } ^{\circ}C) \quad (2)$$

624 Equation 1 was derived for most samples except those from cold seasons, and Equation 2 was
625 obtained for samples from cold seasons (December–March). Equation 2 was constrained to

626 intersect with Equation 1 at -20°C , as there were no significant differences at $T < -20^{\circ}\text{C}$, and
627 Equation 1 was used in this range. The agreement between predicted and measured INPs based on
628 these two equations showed improvement compared to using the single-one equation method above
629 (Figure S14S15), better representing the measured INPs across the full measured temperature
630 range (Figure 89). The accurate prediction of the nearly two years of observations of INPs using
631 this single parameterization, rather than requiring multiple n_s -based parameterizations for specific
632 sources, is likely due to the dominance of coarse dust as the primary INP source in this region.
633 Note that the lack of precise parameterization for biological INPs still introduces larger
634 uncertainties in predictions at warm temperature ranges, while applying the two-equation
635 parameterization based on the seasonal signature of biological INPs identified in this study
636 improves the prediction.

637

638 **4 Summary and atmospheric implications**

639 This study comprehensively characterized INPs over a nearly two-year period in the mountainous
640 Upper Colorado River Basin region. The observed average INP concentrations were 0.15 L^{-1} at
641 -15°C and 16 L^{-1} at -25°C . Clear seasonal variations of INP concentrations and temperature
642 spectra were observed, with low concentrations in winter, increasing in spring, peaking in summer,
643 decreasing in autumn, and returning to low levels in winter. At warm activation temperatures (-10°C
644 to -15°C), some distinct peaks occurred sporadically (i.e., not observed in both years), which were
645 mainly impacted by biological INP emission events. INPs active at colder temperatures showed
646 more repeatable seasonal patterns and were related to the presence of dust and biomass burning
647 aerosols. The aerosol types in this region were identified as coarse dust, fine dust, biomass burning,
648 sulfate-dominated, and nitrate-dominated. Coarse dust concentrations were strongly correlated

649 with INP concentrations in all seasons and over a large temperature range, suggesting that
650 background INPs in the study region were strongly influenced by coarse dust. Further analysis of
651 the IN active surface density site supported the dominant role of coarse dust in INPs. Abundant
652 organic INPs were identified, suggesting that organic-containing soil dust was the primary source
653 of INPs. Back trajectories showed that coarse dust mostly originated from local or regional sources.
654 This study also found clear evidence of biological and heat-labile INPs, which showed strong
655 seasonal dependence. Heat-labile, presumably biological INPs were present during warm seasons
656 but were significantly decreased in winter. Two parameterization equations based on IN active
657 surface site density were developed for warm and cold seasons separately. These equations well
658 estimated the measured INP concentrations across the measured temperature and concentration
659 ranges. The parameterization developed here could be useful for representing INPs from organic-
660 containing soil dust in other mountain regions.

661 The aerosol types in this region were identified as coarse dust, fine dust, biomass burning, sulfate-
662 dominated, and nitrate dominated. Coarse dust concentrations were strongly correlated with INP
663 concentrations in all seasons and over a large temperature range, suggesting that background INPs
664 in the study region were strongly influenced by this aerosol type. Further normalizing by surface
665 area, n_s values supported that the identified aerosol types were related to INP sources, and that
666 coarse dust had a significant impact on INPs. A correlation was found between the concentrations
667 of organic and inorganic INPs observed during SAIL, indicating their similar origins. Specifically,
668 the high ratio between organic and inorganic INP types indicated that organics dominated the INPs,
669 suggesting that organic-containing soil dust was associated with the coarse dust type and was the
670 primary source of INPs. This long-term observation identified that organic-containing soil dust is
671 the major source of INPs in the Rocky Mountain region. Back trajectories showed that coarse dust

672 mostly originated from local or regional sources. Our results indicate that soil dust from nearby
673 regions (e.g., the Colorado Plateau and Central Rockies), rather than long-range transported fine
674 and mineral dust, dominates contributions to the INPs in the Upper Colorado River Basin, and
675 therefore influences aerosol-cloud interaction and precipitation. During events in which aerosols
676 were dominated by biomass burning aerosols and fine dust, likely from long-range transport,
677 play less important roles in INPs compared to coarse dust in this region., aerosol loading and total
678 particle surface area were significantly increased. INP concentrations, especially at lower
679 temperatures, also increased due to contributions from biomass burning aerosols and/or co-emitted
680 dust. Fine dust, likely from long-range transport, showed a weak correlation with INP
681 concentrations, suggesting its limited contribution to INPs. Our results indicate that soil dust from
682 nearby regions (e.g., the Colorado Plateau and Central Rockies), rather than long-range transported
683 fine and mineral dust, dominates contributions to the INPs in the Upper Colorado River Basin, and
684 therefore influences aerosol-cloud interaction and precipitation. This study investigated the major
685 INP sources by linking long-term INP measurements with aerosol source apportionment,
686 presenting reasonable results that agree well with other studies (DeMott et al., 2025; Lacher et al.,
687 2025). This approach may have broader applicability for INP source attribution in other regions.
688 Future studies combining short-term online INP measurement (e.g., continuous flow diffusion
689 chamber, CFDC) with detailed chemical analyses (e.g., mass spectrometer) would be valuable for
690 providing more direct evidence of INP sources, such as demonstrated by the approaches used in
691 Cornwell et al. (2023, 2024).
692 This study also found clear evidence of biological and heat-labile INPs, which showed strong
693 seasonal dependence. Heat-labile, presumably biological INPs were present during warm seasons
694 but were significantly decreased in winter, consistent with the temperature dependence of

695 ~~biological emissions. A correlation was observed between biological/heat-labile INPs and other~~
696 ~~organic INPs at -15°C , while the correlation is weaker at -12.5°C . Tracking or parameterizing~~
697 ~~biological INPs using physical or chemical parameters remains a challenge in INP studies~~
698 ~~(Burrows et al., 2022). The correlation found here could provide insights for estimating biological~~
699 ~~INPs if their sources are better constrained at different active temperatures.~~

700 In this study, the origins of biological INPs are unclear due to the limitations of the analytical
701 methods used. One possibility is that biological INPs were associated with soil dust, e.g., fungi in
702 soil (Conen and Yakutin, 2018; O'Sullivan et al., 2016). This is supported by the correlation
703 between biological/heat-labile INPs and other organic INPs at -15°C . Also, raindrop impact could
704 be an important biological INP emission pathway (Prenni et al., 2013; Mignani et al., 2025). In
705 cold seasons, snow covers the Rocky Mountain region and inhibits the suspension of local soil
706 dust, which is considered as the main source of INPs in this region. This assumption that coarse
707 dust emissions are suppressed in cold seasons is also supported by the observation that more than
708 half of the samples in cold seasons were dominated by mixed sources and fine dust, instead of
709 coarse dust. However, the correlation between biological/heat-labile INPs and other organic INPs
710 was weaker ($R^2 = 0.10$) at a warmer temperature (-12.5°C). This suggests that there are
711 contributions from other biological INPs (e.g., those originating from vegetation) at warmer
712 freezing temperatures, which are likely independent of soil dust emissions, thereby complicating
713 the estimation of biological INPs. For example, airborne bacteria (Bowers et al., 2012) and pollen
714 (Fall et al., 1992) in the Rocky Mountain region decrease in winter and increase during the warmer
715 seasons. This seasonal pattern is consistent with the variation in biological/heat-labile INPs
716 observed in this study, suggesting that these biological particles may represent potential sources of
717 the biological INPs. In this case, the INP spectra in cold seasons likely represent that of soil dust,

718 and the spectra in other seasons represent the combination of soil dust and biological INPs. While
719 bacteria may also be partly related to soil, as summer bacteria taxa were reported to likely originate
720 from soil and leaf surface (Bowers et al., 2012), the specific ice-active taxa among them require
721 further investigation. In future studies, identifying whether biological INPs originate from
722 vegetation, from soil associated sources, or from a combination of both, and clarifying their
723 relative contributions, would help improve our understanding of biological INP variability and
724 could potentially improve their estimation. In future studies, identifying the most abundant
725 biological INPs in this region and determining whether they originate from vegetation, soil-
726 associated sources, or from a combination of both would help improve our understanding of
727 biological INP variability and improve their estimation. However, besides heat treatment, current
728 approaches provide only indirect evidence of biological INPs (Cornwell et al., 2023 and 2024;
729 Sanchez-Marroquin et al., 2021). Comprehensive characterization of biological aerosol types and
730 abundance, or developing new analytical approaches, would be highly beneficial for advancing
731 biological INP research.

732 ~~Based on the seasonal variation of heat labile and biological INPs, two separate parameterization~~
733 ~~equations based on IN active surface site density were developed for warm and cold seasons. These~~
734 ~~equations well estimated the measured INP concentrations across the measured temperature and~~
735 ~~concentration ranges. The parameterization developed here could be useful for representing INPs~~
736 ~~from organic containing soil dust in other mountain regions. Furthermore, + The INP concentrations~~
737 in this study were similar to those observed in ambient samples influenced by agricultural soil in
738 Argentina (Testa et al., 2021). The n_s values reported for agricultural soil samples (Tobo et al.,
739 2014) were higher than those calculated from total surface area (Figure S15S10), but similar to n_s
740 when based on surface area of particles > 500 nm (Figure S13S14). This finding suggests that

741 using particles > 500 nm is a reasonable threshold for excluding most aerosol types that are
742 inefficient INP sources, and approximating aerosol surface area contributions from organic-
743 containing soils. Since SAIL was conducted at a remote site in the Rocky Mountains, these
744 comparisons suggest that the parameterization developed in this study can potentially be applied
745 to other remote continental areas. A recent global modeling study (Herbert et al., 2025) found that
746 including organic INP components in dust particles, which are present in many soils, can
747 significantly improve predictive accuracy. It is therefore essential to validate the INPs originating
748 from organic-containing soil dust, beyond the mineral dust that has already been intensively
749 studied, through field measurements across different continental regions.

750

751 **Data Availability**

752 The data from the SAIL campaign used in this study are available through the ARM Data
753 Discovery (<https://adc.arm.gov/discovery/>). This includes INPs data (Shi et al., 2025), source
754 apportionment results (Zhou et al., 2025a), back trajectory data (Zhou et al., 2025b), merged
755 aerosol number-size distribution (Zhou et al., 2025c), and particle number size distribution data
756 from SMPS (Kuang et al., 2024) and OPC (Cromwell et al., 2024).

757

758 **Author contributions**

759 RP, SK, PD, and RZ conceptualized the study. DJ, RZ, KA, and OD performed additional
760 immersion-mode INP measurements. RZ, RP and SK conducted the source apportionment and
761 merged the size distribution data. RZ, RP, KA and SK performed the back trajectory analysis. KB

762 performed qPCR analysis. RZ wrote the manuscript, with revisions from RP, PD, and SK. All
763 authors reviewed the manuscript and contributed to the final version of the manuscript.

764

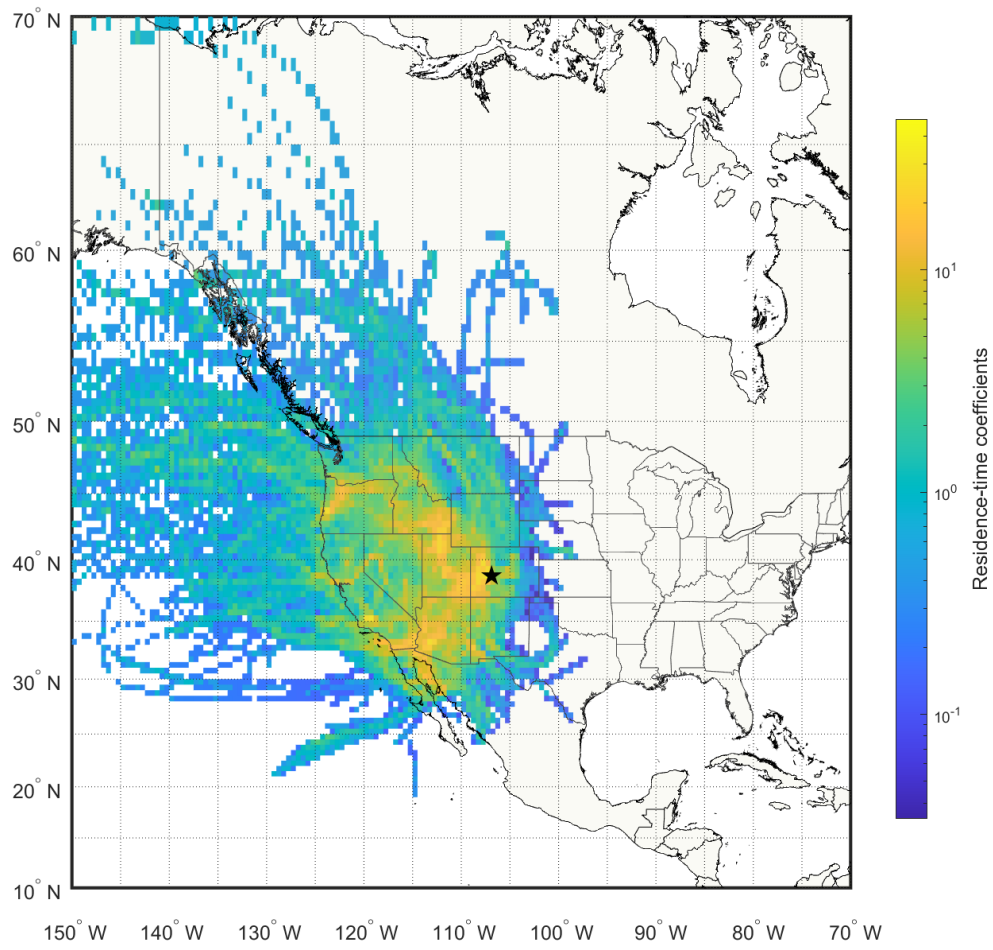
765 **Competing interests**

766 The authors declare no competing interests.

767

768 **Acknowledgements**

769 This work is supported by DOE Atmospheric Systems Research award DE-SC0024202 and DE-
770 SC0021116. We thank the DOE ARM INP Mentors Jessie Creamean, Tom Hill, and Carson Hume
771 for coordinating the sample collections and for helping with the combined INP data archival. We
772 also thank Ty Johnson for assistance with generating the NOAA Hazard Mapping System plots.
773 The authors acknowledge the NOAA Air Resources Laboratory (ARL) for the provision of the
774 HYSPLIT transport and dispersion model used in this publication. We also thank the Interagency
775 Monitoring of Protected Visual Environments (IMPROVE) network for providing aerosol
776 composition data. IMPROVE is a collaborative association of state, tribal, and federal agencies,
777 and international partners. US Environmental Protection Agency is the primary funding source,
778 with contracting and research support from the National Park Service. The Air Quality Group at
779 the University of California, Davis is the central analytical laboratory, with ion analysis provided
780 by Research Triangle Institute, and carbon analysis provided by Desert Research Institute. We
781 thank North American Weather Consultants Inc. for providing records of their cloud seeding
782 activities near the SAIL campaign site. Kelton Ayars and Oren Dutton would like to acknowledge
783 support from the Scott Undergraduate Research Experiences program at Colorado State University.



784

785 **Figure 1.** Residence-time weighted back trajectories for all sampling periods. 96-hour back
 786 trajectories were generated hourly during each sampling period and normalized by residence
 787 time and distance from the sampling site. The residence-time coefficients indicate the relative
 788 time air masses spent within each grid cell. The black star marks the SAIL sampling location.

789

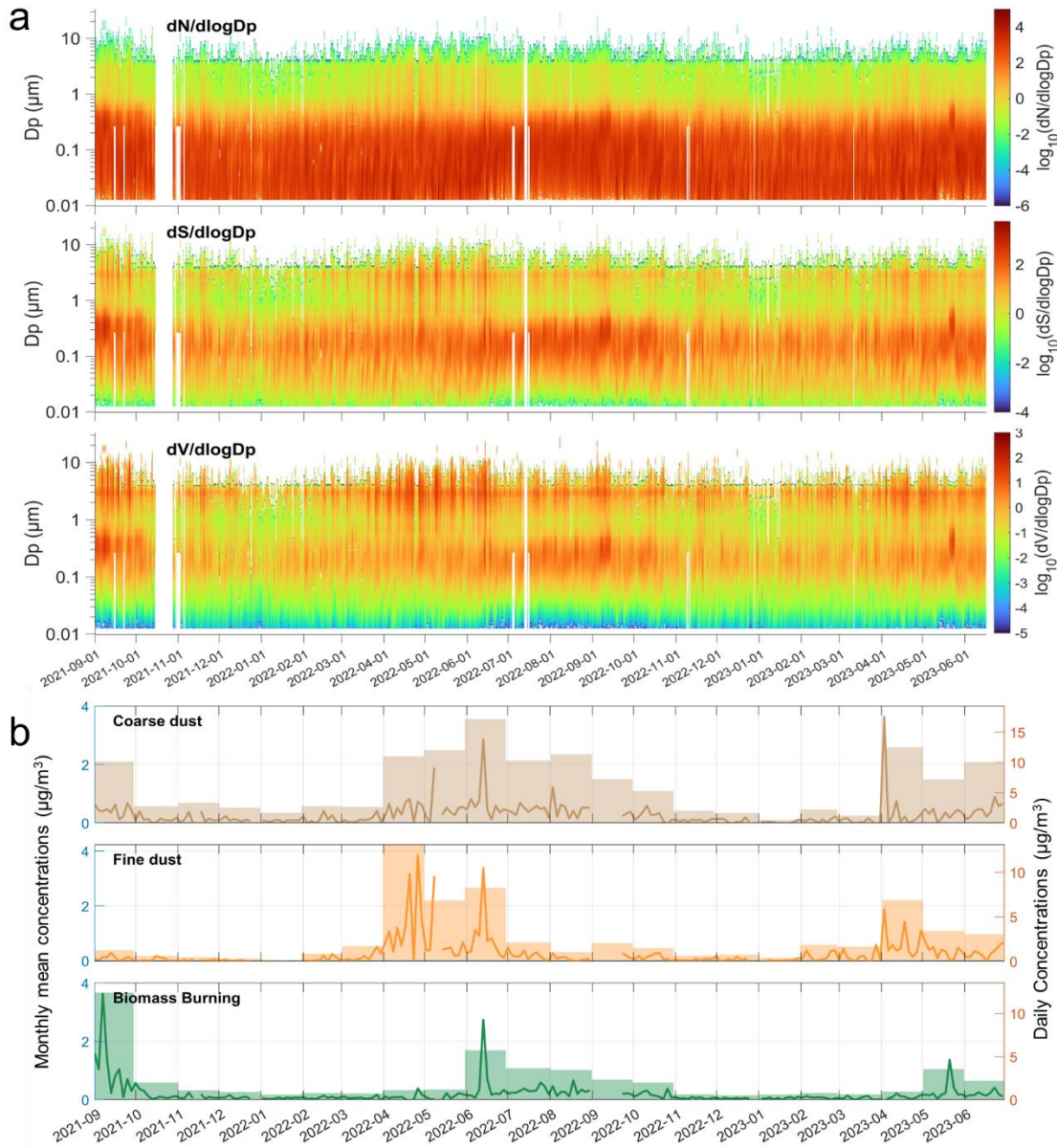
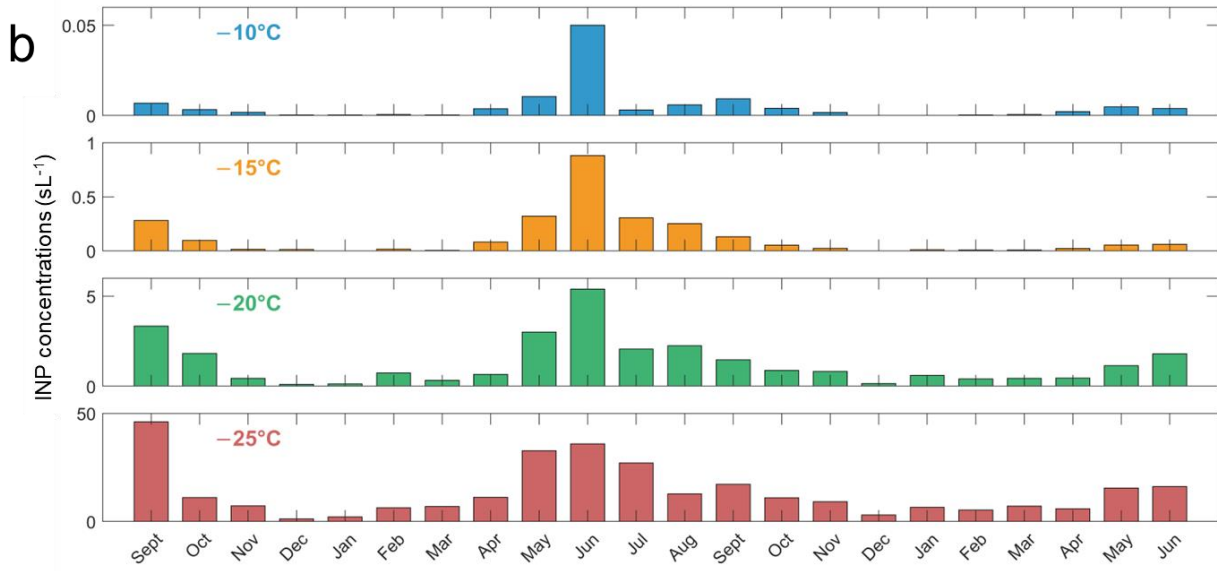
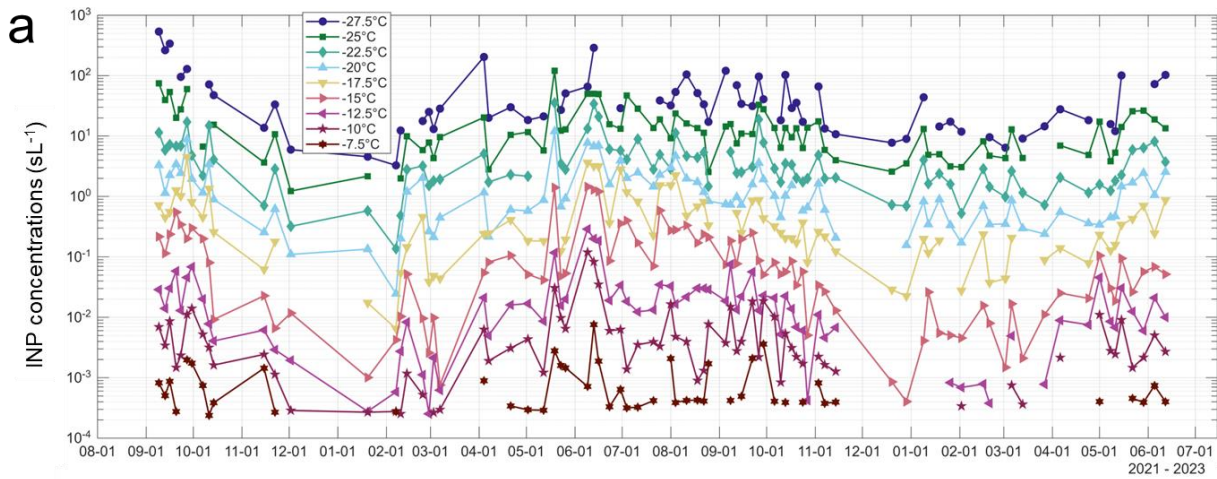
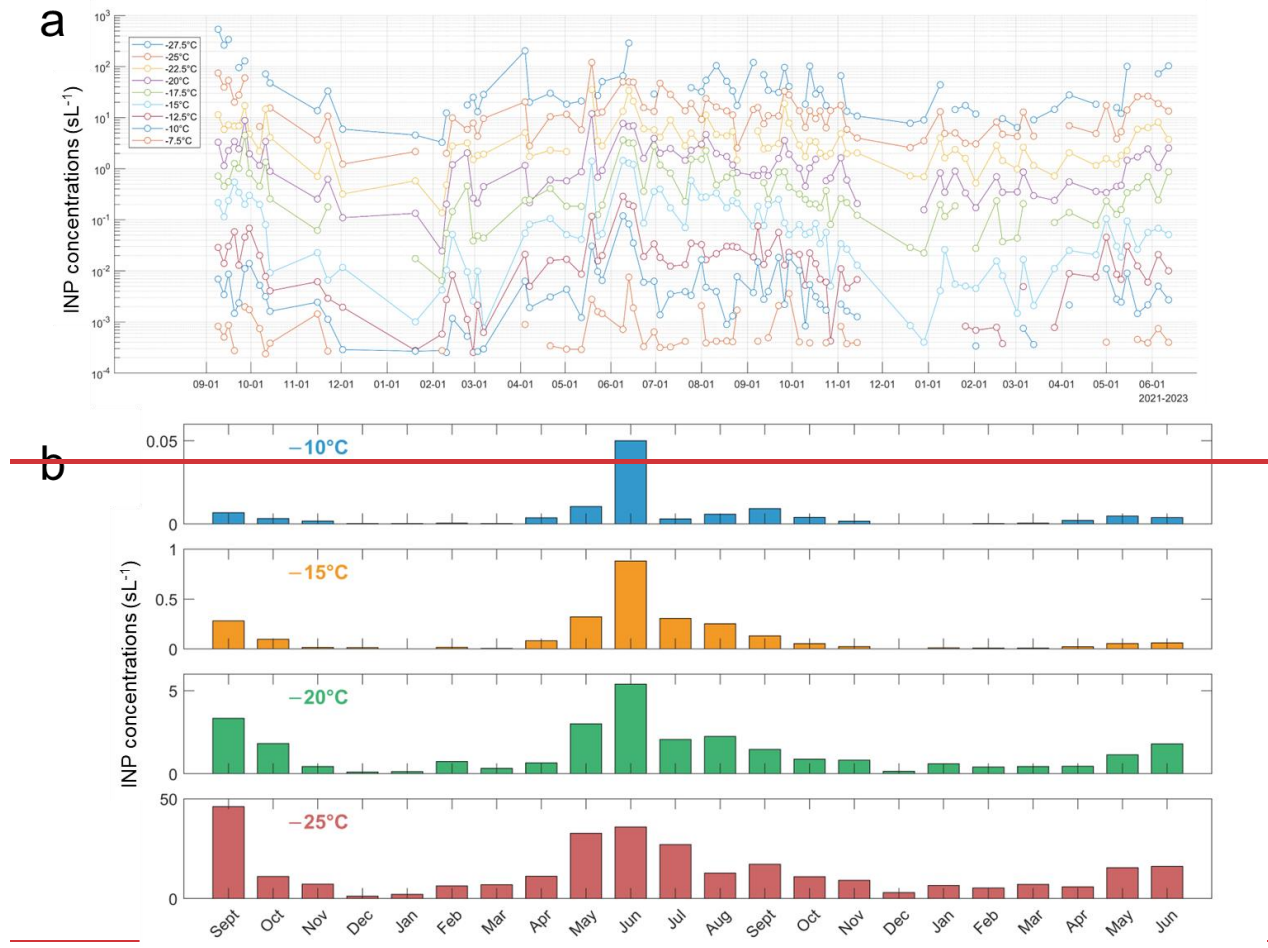
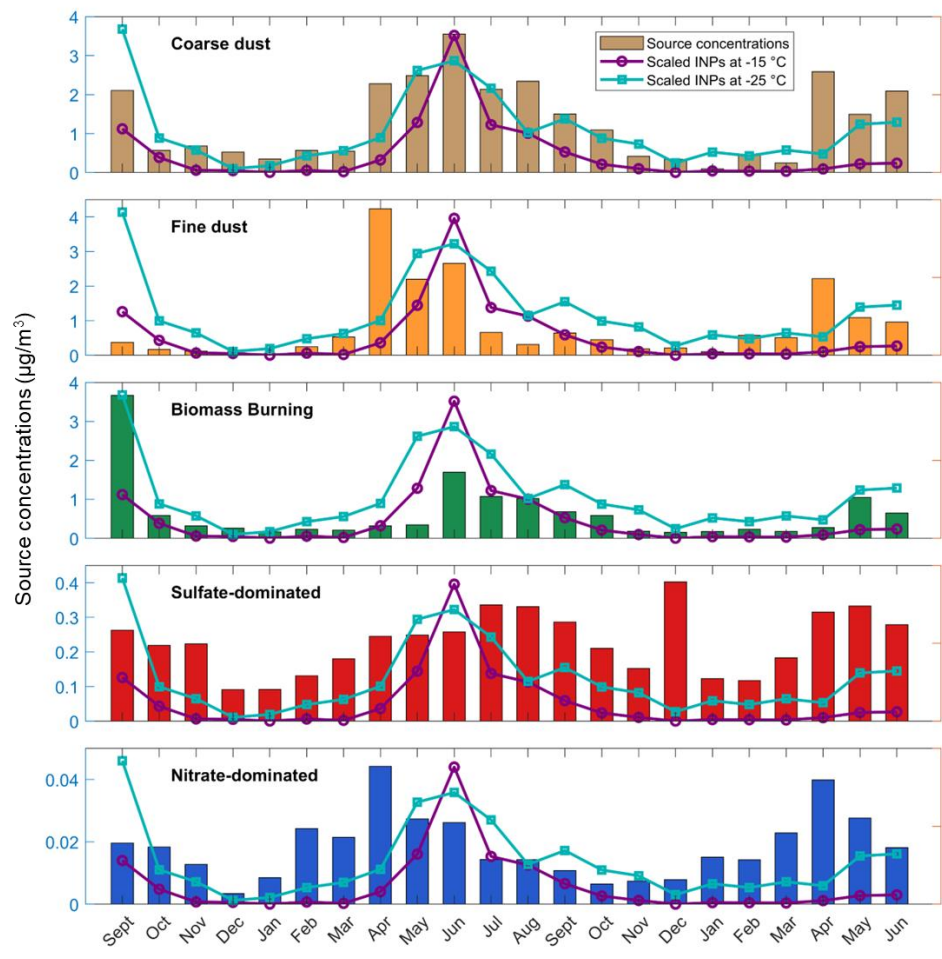


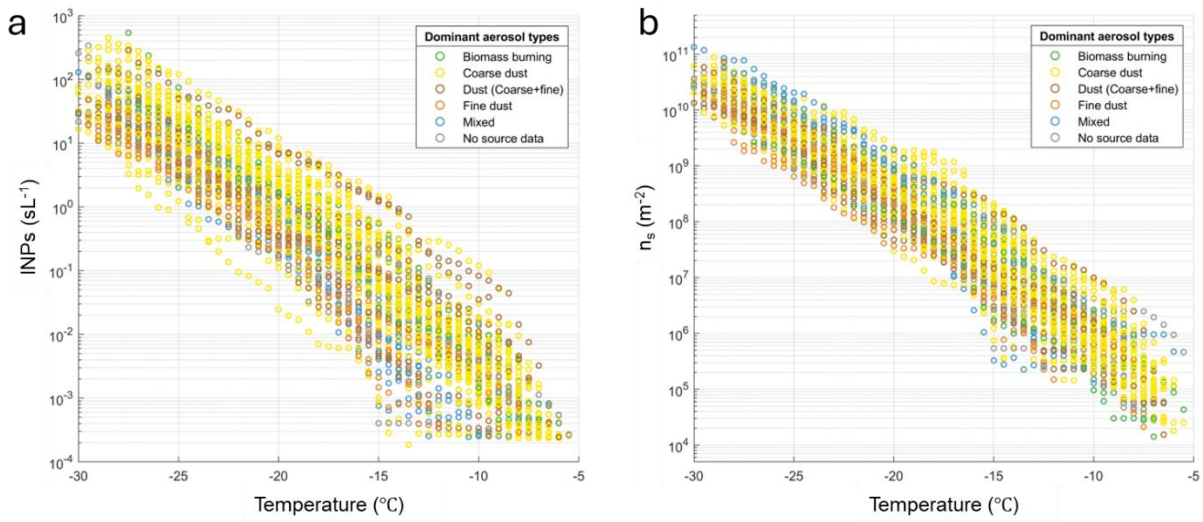
Figure 2. (a) Number size distribution ($dN/d\log D_p$, scm^{-3}), surface area size distribution ($dS/d\log D_p$, $\mu\text{m}^2/\text{scm}^{-3}$), and volume size distribution ($dV/d\log D_p$, $\mu\text{m}^3/\text{scm}^{-3}$), derived from merged size distribution assuming spherical particles during the SAIL campaign. (b) Time series of aerosol mass concentrations ($\mu\text{g m}^{-3}$) of coarse dust, fine dust, and biomass burning. Lines and bars represent daily and monthly mean concentrations, respectively.







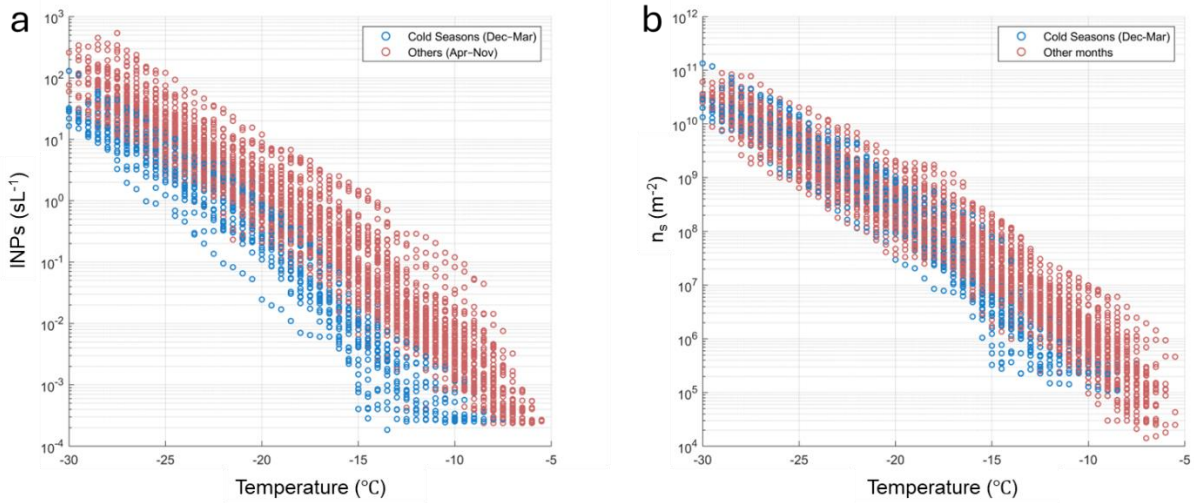
803
804 **Figure 4.** Monthly mean INP concentrations (lines, arbitrary scaling) at -15°C and -25°C and
805 monthly mean aerosol mass concentrations (bars) from coarse dust, fine dust, biomass burning,
806 sulfate-dominated, and nitrate-dominated sources.
807



808

809 **Figure 45.** (a) Total INP concentration (sL^{-1}) temperature spectra, and (b) IN active surface site
 810 density (n_s, m^{-2}) calculated based on the surface area of particles larger than 500 nm. All samples
 811 were categorized by the dominant aerosol sources. Colors in the legend represent the dominant
 812 aerosol types during sampling.

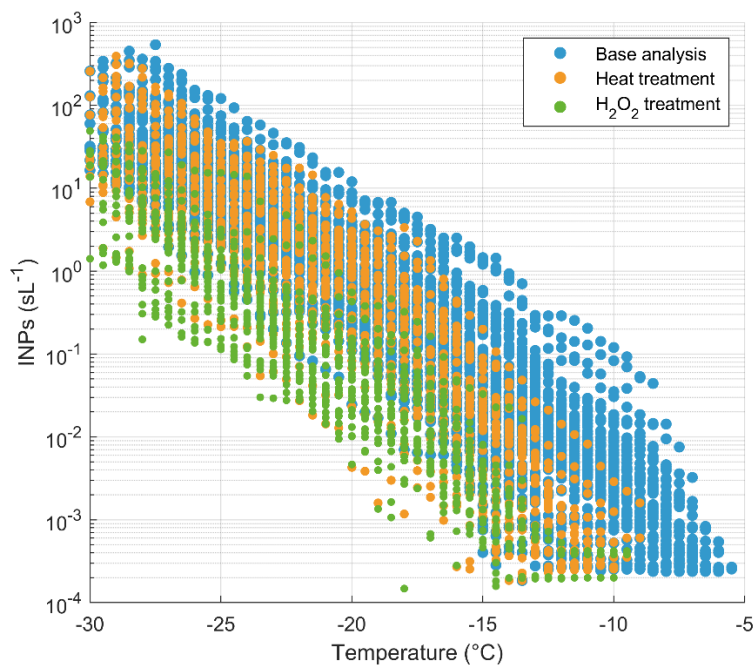
813



814

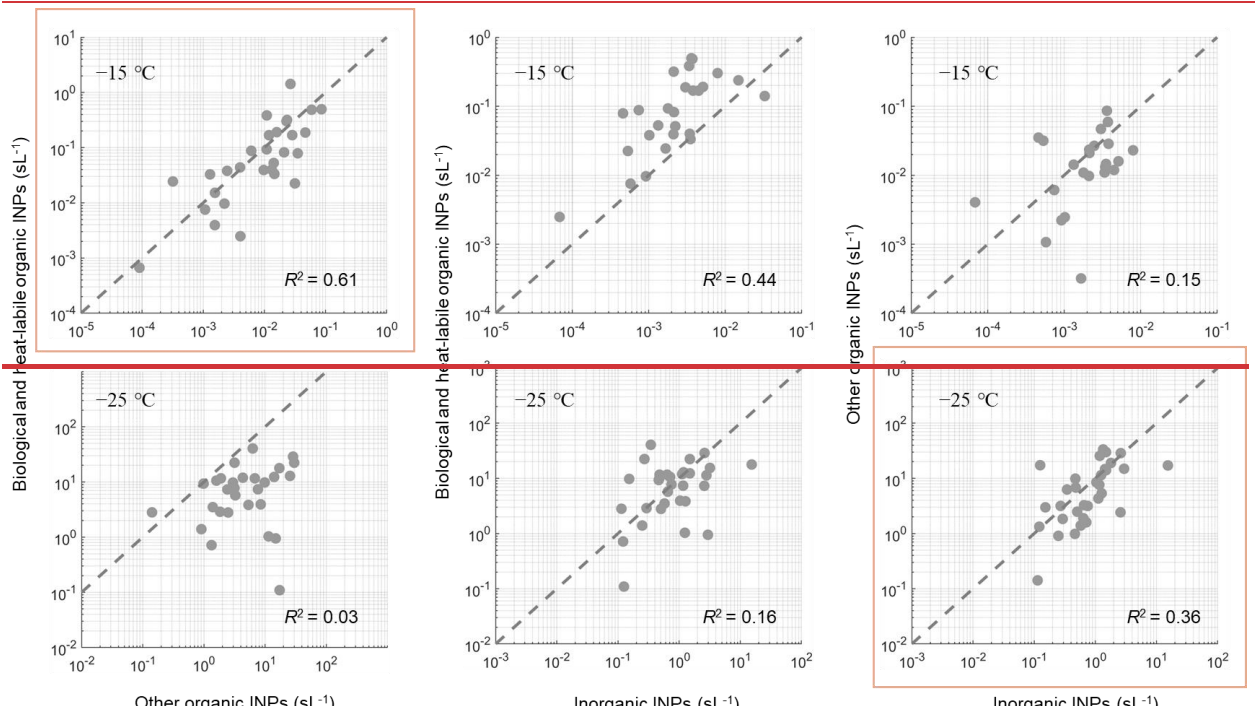
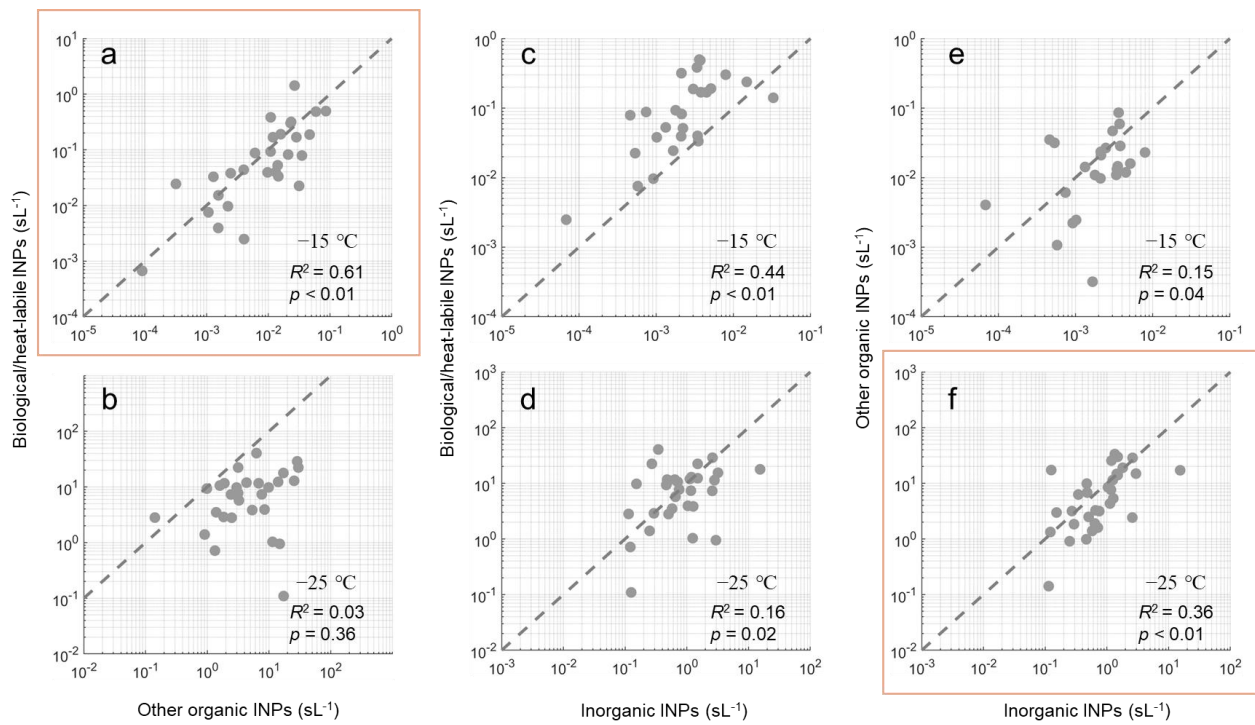
815 **Figure 56.** (a) INP temperature spectra and (b) IN active surface site density (n_s) categorized by
 816 sampling date as cold seasons (December–March) and other seasons (April–November). n_s was
 817 calculated based on the surface area of particles larger than 500 nm.

818



819

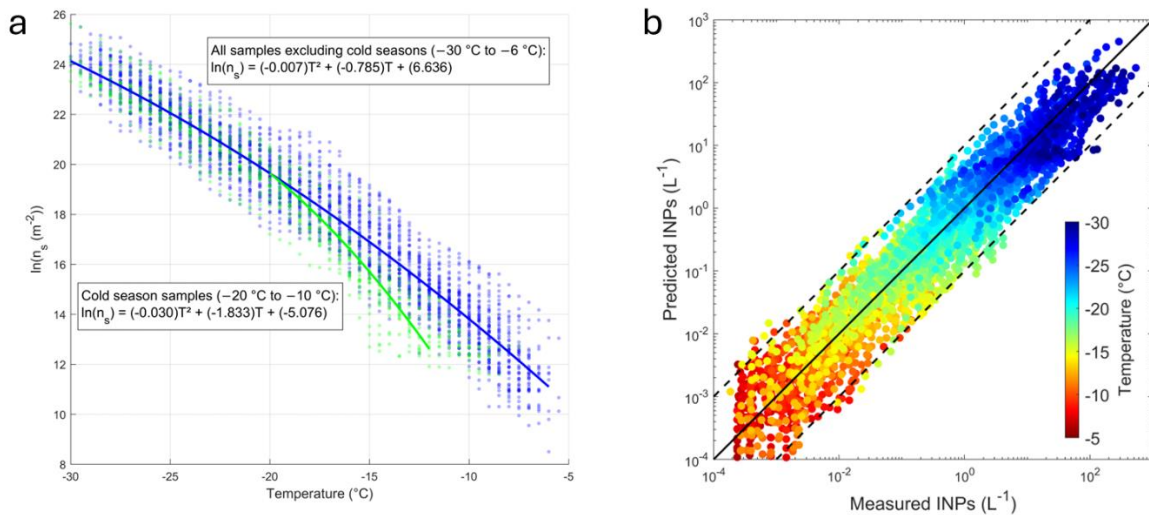
820 **Figure 67.** Comparison of INP temperature spectra from base (untreated), heat-treated, and
 821 H_2O_2 -treated analyses.



824 **Figure 78.** Correlations between concentrations of (a, b) biological/heat-labile
825 INPs, and other organic INPs, (c, d) biological/heat-labile INPs and inorganic INPs, and (e, f)
826 other organic INPs and inorganic INPs, active at either temperatures of -15 °C (upper
827 row) and/or -25 °C (lower row). Dashed lines show indicate a 10:1 correlation relationship for

828 reference, and, ~~T~~ the orange rectangles ~~show~~highlight the ~~highest~~strongest correlations at each
829 temperature.

830



831
832 **Figure 89.** (a) All cold season (December–March) and other seasons (April–November) INP
833 data, expressed as IN active surface site density n_s (based on the surface area of particles larger
834 than 500 nm), with parameterization fits. All samples, excluding those from cold seasons, were
835 used to develop the parameterization equation for temperatures from -30°C to -6°C . A separate
836 equation was developed for samples from cold seasons at temperatures from -20°C to -10°C .
837 (b) Comparison between predicted INP concentrations based on the parameterization equations
838 and measured surface area concentrations, and measured INP concentrations.

839

840 **Table 1.** Pearson correlation coefficients (R^2) between monthly means of INP concentrations and
841 source factor concentrations.

	Coarse dust	Fine dust	Biomass burning	Sulfate-dominated	Nitrate-dominated	Coarse dust and biomass burning
-10 °C	0.430*	0.192	0.157	0.070	0.036	0.389*
-15 °C	0.568*	0.175	0.316*	0.093	0.040	0.590*
-20 °C	0.579*	0.117	0.484*	0.121	0.040	0.706*
-25 °C	0.500*	0.100	0.688*	0.147	0.051	0.763*

842 * p < 0.01

843

844 References

845 Agresti, A. and Coull, B. A.: Approximate is better than “exact” for interval estimation of
846 binomial proportions, *Am. Stat.*, 52, 119-126, 1998.

847 Ashbaugh, L. L., Malm, W. C., and Sadeh, W. Z.: A residence time probability analysis of sulfur
848 concentrations at Grand Canyon National Park, *Atmos. Environ.*, 19, 1263-1270, 1985.

849 Atkinson, J. D., Murray, B. J., Woodhouse, M. T., Whale, T. F., Baustian, K. J., Carslaw, K. S.,
850 Dobbie, S., O’Sullivan, D., and Malkin, T. L.: The importance of feldspar for ice nucleation by
851 mineral dust in mixed-phase clouds, *Nature*, 498, 355-358, <https://doi.org/10.1038/nature12278>,
852 2013.

853 Barry, K. R., Hill, T. C. J., Jentzsch, C., Moffett, B. F., Stratmann, F., and DeMott, P. J.:
854 Pragmatic protocols for working cleanly when measuring ice nucleating particles, *Atmos. Res.*,
855 250, <https://doi.org/10.1016/j.atmosres.2020.105419>, 2021a.

856 Barry, K. R., Hill, T. C. J., Levin, E. J. T., Twohy, C. H., Moore, K. A., Weller, Z. D., Toohey, D.
857 W., Reeves, M., Campos, T., Geiss, R., Schill, G. P., Fischer, E. V., Kreidenweis, S. M., and
858 DeMott, P. J.: Observations of Ice Nucleating Particles in the Free Troposphere From Western
859 US Wildfires, *J. Geophys. Res: Atmos.*, 126, <https://doi.org/10.1029/2020jd033752>, 2021b.

860 Beall, C. M., Hill, T. C. J., DeMott, P. J., Köneman, T., Pikridas, M., Drewnick, F., Harder, H.,
861 Pöhlker, C., Lelieveld, J., Weber, B., Iakovides, M., Prokes, R., Sciare, J., Andreae, M. O.,
862 Stokes, M. D., and Prather, K. A.: Ice-nucleating particles near two major dust source regions,
863 *Atmos. Chem. Phys.*, 22, 12607-12627, <https://doi.org/10.5194/acp-22-12607-2022>, 2022.

864 Bigg, E. K.: The supercooling of water, *Proceedings of the Physical Society. Section B*, 66, 688,
865 1953.

866 [Bowers, R. M., McCubbin, I. B., Hallar, A. G., and Fierer, N.: Seasonal variability in airborne
867 bacterial communities at a high-elevation site, *Atmos. Environ.*, 50, 41-49,
868 <https://doi.org/10.1016/j.atmosenv.2012.01.005>, 2012.](https://doi.org/10.1016/j.atmosenv.2012.01.005)

869 [Brown, S. G., Eberly, S., Paatero, P., and Norris, G. A.: Methods for estimating uncertainty in
870 PMF solutions: examples with ambient air and water quality data and guidance on reporting
871 PMF results, *Sci. Total Environ.*, 518-519, 626-635,
872 <https://doi.org/10.1016/j.scitotenv.2015.01.022>, 2015.](https://doi.org/10.1016/j.scitotenv.2015.01.022)

873 Burrows, S. M., McCluskey, C. S., Cornwell, G., Steinke, I., Zhang, K., Zhao, B., Zawadowicz,
874 M., Raman, A., Kulkarni, G., and China, S.: Ice-nucleating particles that impact clouds and
875 climate: Observational and modeling research needs, *Rev. Geophys.*, 60, e2021RG000745, 2022.

876 Conen, F. and Yakutin, M. V.: Soils rich in biological ice-nucleating particles abound in ice-
877 nucleating macromolecules likely produced by fungi, *Biogeosciences*, 15, 4381-4385,
878 <https://doi.org/10.5194/bg-15-4381-2018>, 2018.

879 Conen, F., Rodríguez, S., Hulin, C., Henne, S., Herrmann, E., Bukowiecki, N., and Alewell, C.:
880 Atmospheric ice nuclei at the high-altitude observatory Jungfraujoch, Switzerland, *Tellus B
881 Chem. Phys. Meteorol.*, 67, 25014, 2015.

882 Creamean, J. M., Hill, T. C., Hume, C. C., and Devadoss, T.: Ice Nucleation Spectrometer (INS)
883 Instrument Handbook, Oak Ridge National Laboratory (ORNL), Oak Ridge, TN (United States)

884 Atmospheric Radiation Measurement (ARM) Data Center, <https://doi.org/10.2172/1846263>,
885 2024.

886 Creamean, J. M., Suski, K. J., Rosenfeld, D., Cazorla, A., DeMott, P. J., Sullivan, R. C., White,
887 A. B., Ralph, F. M., Minnis, P., and Comstock, J. M.: Dust and biological aerosols from the
888 Sahara and Asia influence precipitation in the western US, *Science*, 339, 1572-1578, 2013.

889 [Cornwell, G. C., McCluskey, C. S., Hill, T. C. J., Levin, E. T., Rothfuss, N. E., Tai, S. L., Petters, M. D., DeMott, P. J., Kreidenweis, S., Prather, K. A., and Burrows, S. M.: Bioaerosols are the dominant source of warm-temperature immersion-mode INPs and drive uncertainties in INP predictability, Sci Adv, 9, eadg3715, https://doi.org/10.1126/sciadv.adg3715, 2023.](#)

890 [Cornwell, G. C., Steinke, I., Lata, N. N., Zelenyuk, A., Kulkarni, G., Pekour, M., Perkins, R., Levin, E. J. T., China, S., Demott, P. J., and Burrows, S. M.: Enrichment of Phosphates, Lead, and Mixed Soil-Organic Particles in INPs at the Southern Great Plains Site, J. Geophys. Res: Atmos., 129, https://doi.org/10.1029/2024jd040826, 2024.](#)

891 [Cornwell, G. C., Steinke, I., Lata, N. N., Zelenyuk, A., Kulkarni, G., Pekour, M., Perkins, R., Levin, E. J. T., China, S., Demott, P. J., and Burrows, S. M.: Enrichment of Phosphates, Lead, and Mixed Soil-Organic Particles in INPs at the Southern Great Plains Site, J. Geophys. Res: Atmos., 129, https://doi.org/10.1029/2024jd040826, 2024.](#)

892 [Cornwell, G. C., Steinke, I., Lata, N. N., Zelenyuk, A., Kulkarni, G., Pekour, M., Perkins, R., Levin, E. J. T., China, S., Demott, P. J., and Burrows, S. M.: Enrichment of Phosphates, Lead, and Mixed Soil-Organic Particles in INPs at the Southern Great Plains Site, J. Geophys. Res: Atmos., 129, https://doi.org/10.1029/2024jd040826, 2024.](#)

893 Cromwell, E., Singh, A., & Kuang, C. Optical Particle Counter (AOSOPC), 2021-10-27 to 2023-06-16, ARM Mobile Facility (GUC), Gunnison, CO; Supplemental Facility 2 (S2). Atmospheric Radiation Measurement (ARM) User Facility. <https://doi.org/10.5439/1824224>, Data accessed 2024-08-01.

901 de Boer, G., Morrison, H., Shupe, M. D., and Hildner, R.: Evidence of liquid dependent ice
902 nucleation in high-latitude stratiform clouds from surface remote sensors, *Geophys. Res. Lett.*,
903 38, 2011.

904 DeMott, P. J., Sassen, K., Poellot, M. R., Baumgardner, D., Rogers, D. C., Brooks, S. D., Prenni,
905 A. J., and Kreidenweis, S. M.: African dust aerosols as atmospheric ice nuclei, *Geophys. Res. Lett.*,
906 30, <https://doi.org/10.1029/2003gl017410>, 2003.

907 DeMott, P. J., Prenni, A. J., Liu, X., Kreidenweis, S. M., Petters, M. D., Twohy, C. H.,
908 Richardson, M. S., Eidhammer, T., and Rogers, D. C.: Predicting global atmospheric ice nuclei
909 distributions and their impacts on climate, *Proc. Natl. Acad. Sci. USA*, 107, 11217-11222,
910 <https://doi.org/10.1073/pnas.0910818107>, 2010.

911 DeMott, P. J., Prenni, A. J., McMeeking, G. R., Sullivan, R. C., Petters, M. D., Tobe, Y.,
912 Niemand, M., Möhler, O., Snider, J. R., Wang, Z., and Kreidenweis, S. M.: Integrating laboratory
913 and field data to quantify the immersion freezing ice nucleation activity of mineral dust particles,
914 *Atmos. Chem. Phys.*, 15, 393-409, <https://doi.org/10.5194/acp-15-393-2015>, 2015.

915 DeMott, P. J., Mirrieles, J. A., Petters, S. S., Cziczo, D. J., Petters, M. D., Bingemer, H. G., Hill,
916 T. C. J., Froyd, K., Garimella, S., Hallar, A. G., Levin, E. J. T., McCubbin, I. B., Perring, A. E.,
917 Rapp, C. N., Schiebel, T., Schrod, J., Suski, K. J., Weber, D., Wolf, M. J., Zawadowicz, M.,
918 Zenker, J., Möhler, O., and Brooks, S. D.: Field intercomparison of ice nucleation measurements:
919 the Fifth International Workshop on Ice Nucleation Phase 3 (FIN-03), *Atmos. Meas. Tech.*, 18,
920 639-672, <https://doi.org/10.5194/amt-18-639-2025>, 2025.

921 Després, V., Huffman, J. A., Burrows, S. M., Hoose, C., Safatov, A., Buryak, G., Fröhlich-
922 Nowoisky, J., Elbert, W., Andreae, M., Pöschl, U., and Jaenicke, R.: Primary biological aerosol
923 particles in the atmosphere: a review, *Tellus B Chem. Phys. Meteorol.*, 64, 15598,
924 <https://doi.org/10.3402/tellusb.v64i0.15598>, 2012.

925 Fall, P. L.: [Spatial patterns of atmospheric pollen dispersal in the Colorado Rocky Mountains, USA, Review of Palaeobotany and Palynology, 74, 293-313, https://doi.org/10.1016/0034-6667\(92\)90013-7, 1992.](#)

928 Feldman, D. R., Aiken, A. C., Boos, W. R., Carroll, R. W. H., Chandrasekar, V., Collis, S.,
929 Creamean, J. M., de Boer, G., Deems, J., DeMott, P. J., Fan, J., Flores, A. N., Gochis, D., Grover,
930 M., Hill, T. C. J., Hodshire, A., Hulm, E., Hume, C. C., Jackson, R., Junyent, F., Kennedy, A.,
931 Kumjian, M., Levin, E. J. T., Lundquist, J. D., O'Brien, J., Raleigh, M. S., Reithel, J., Rhoades,
932 A., Rittger, K., Rudisill, W., Sherman, Z., Siirila-Woodburn, E., Skiles, S. M., Smith, J. N.,
933 Sullivan, R. C., Theisen, A., Tuftedal, M., Varble, A. C., Wiedlea, A., Wielandt, S., Williams, K.,
934 and Xu, Z.: The Surface Atmosphere Integrated Field Laboratory (SAIL) Campaign, *Bull. Amer. Meteor. Soc.*, 104, E2192-E2222, <https://doi.org/10.1175/bams-d-22-0049.1>, 2023.

936 Fröhlich-Nowoisky, J., Kampf, C. J., Weber, B., Huffman, J. A., Pöhlker, C., Andreae, M. O.,
937 Lang-Yona, N., Burrows, S. M., Gunthe, S. S., and Elbert, W.: Bioaerosols in the Earth system:
938 Climate, health, and ecosystem interactions, *Atmos. Res.*, 182, 346-376, 2016.

939 Garcia, E., Hill, T. C., Prenni, A. J., DeMott, P. J., Franc, G. D., and Kreidenweis, S. M.:
940 Biogenic ice nuclei in boundary layer air over two US High Plains agricultural regions, *J. Geophys. Res: Atmos.*, 117, 2012.

942 Ginoux, P., Prospero, J. M., Gill, T. E., Hsu, N. C., and Zhao, M.: Global-scale attribution of
943 anthropogenic and natural dust sources and their emission rates based on MODIS Deep Blue
944 aerosol products, *Rev. Geophys.*, 50, <https://doi.org/10.1029/2012rg000388>, 2012.

945 Hamzehpour, N., Marcolli, C., Klumpp, K., Thöny, D., and Peter, T.: The Urmia playa as a
946 source of airborne dust and ice-nucleating particles – Part 2: Unraveling the relationship between
947 soil dust composition and ice nucleation activity, *Atmos. Chem. Phys.*, 22, 14931-14956,
948 <https://doi.org/10.5194/acp-22-14931-2022>, 2022.

949 Hand, J. L. and Kreidenweis, S. M.: A New Method for Retrieving Particle Refractive Index and
950 Effective Density from Aerosol Size Distribution Data, *Aerosol Sci. Technol.*, 36, 1012-1026,
951 <https://doi.org/10.1080/02786820290092276>, 2002.

952 Hand, J. L., Gill, T. E., and Schichtel, B. A.: Spatial and seasonal variability in fine mineral dust
953 and coarse aerosol mass at remote sites across the United States, *J. Geophys. Res: Atmos.*, 122,
954 3080-3097, <https://doi.org/10.1002/2016jd026290>, 2017.

955 [Hand, J.: IMPROVE Data User Guide 2023 \(Version 2\), Interagency Monitoring of Protected
956 Visual Environments \(IMPROVE\) Program, available at:
957 <https://vista.cira.colostate.edu/Improve/data-user-guide/>, 2023.](#)

958 Harrison, A. D., Lever, K., Sanchez-Marroquin, A., Holden, M. A., Whale, T. F., Tarn, M. D.,
959 McQuaid, J. B., and Murray, B. J.: The ice-nucleating ability of quartz immersed in water and its
960 atmospheric importance compared to K-feldspar, *Atmos. Chem. Phys.*, 19, 11343-11361,
961 <https://doi.org/10.5194/acp-19-11343-2019>, 2019.

962 Herbert, R. J., Sanchez-Marroquin, A., Grosvenor, D. P., Pringle, K. J., Arnold, S. R., Murray, B.
963 J., and Carslaw, K. S.: Gaps in our understanding of ice-nucleating particle sources exposed by
964 global simulation of the UK Earth System Model, *Atmos. Chem. Phys.*, 25, 291-325, 2025.

965 Hill, T. C. J., DeMott, P. J., Toto, Y., Fröhlich-Nowoisky, J., Moffett, B. F., Franc, G. D., and
966 Kreidenweis, S. M.: Sources of organic ice nucleating particles in soils, *Atmos. Chem. Phys.*, 16,
967 7195-7211, <https://doi.org/10.5194/acp-16-7195-2016>, 2016.

968 Hiranuma, N., Augustin-Bauditz, S., Bingemer, H., Budke, C., Curtius, J., Danielczok, A., Diehl,
969 K., Dreischmeier, K., Ebert, M., Frank, F., Hoffmann, N., Kandler, K., Kiselev, A., Koop, T.,
970 Leisner, T., Möhler, O., Nillius, B., Peckhaus, A., Rose, D., Weinbruch, S., Wex, H., Boose, Y.,
971 DeMott, P. J., Hader, J. D., Hill, T. C. J., Kanji, Z. A., Kulkarni, G., Levin, E. J. T., McCluskey,
972 C. S., Murakami, M., Murray, B. J., Niedermeier, D., Petters, M. D., O'Sullivan, D., Saito, A.,
973 Schill, G. P., Tajiri, T., Tolbert, M. A., Welti, A., Whale, T. F., Wright, T. P., and Yamashita, K.: A
974 comprehensive laboratory study on the immersion freezing behavior of illite NX particles: a
975 comparison of 17 ice nucleation measurement techniques, *Atmos. Chem. Phys.*, 15, 2489-2518,
976 <https://doi.org/10.5194/acp-15-2489-2015>, 2015.

977 Hoose, C. and Möhler, O.: Heterogeneous ice nucleation on atmospheric aerosols: a review of
978 results from laboratory experiments, *Atmos. Chem. Phys.*, 12, 9817-9854,
979 <https://doi.org/10.5194/acp-12-9817-2012>, 2012.

980 [Hopke, P. K., Dai, Q., Li, L., and Feng, Y.: Global review of recent source apportionments for](#)
981 [airborne particulate matter, *Sci. Total Environ.*, 740, 140091,](#)
982 <https://doi.org/10.1016/j.scitotenv.2020.140091>, 2020.

983 Huang, S., Hu, W., Chen, J., Wu, Z. J., Zhang, D. Z., and Fu, P. Q.: Overview of biological ice
984 nucleating particles in the atmosphere, *Environ. Int.*, 146,
985 <https://doi.org/10.1016/j.envint.2020.106197>, 2021.

986 [Hwang, I. and Hopke, P. K.: Estimation of source apportionment and potential source locations](#)
987 [of PM2.5 at a west coastal IMPROVE site, *Atmos. Environ.*, 41, 506-518,](#)
988 <https://doi.org/10.1016/j.atmosenv.2006.08.043>, 2007.

989

990 IPCC, 2022: Climate Change 2022: Impacts, Adaptation, and Vulnerability., Contribution of
991 Working Group II to the Sixth Assessment Report of the Intergovernmental Panel on Climate
992 Change [H.-O. Pörtner, D.C. Roberts, M. Tignor, E.S. Poloczanska, K. Mintenbeck, A. Alegría,
993 M. Craig, S. Langsdorf, S. Löschke, V. Möller, A. Okem, B. Rama (eds.)]. Cambridge University
994 Press. Cambridge University Press, Cambridge, UK and New York, NY, USA, 3056 pp.,
995 <https://doi.org/10.1017/9781009325844>, 2022.

996 Jahl, L. G., Brubaker, T. A., Polen, M. J., Jahn, L. G., Cain, K. P., Bowers, B. B., Fahy, W. D.,
997 Graves, S., and Sullivan, R. C.: Atmospheric aging enhances the ice nucleation ability of
998 biomass-burning aerosol, *Sci. Adv.*, 7, eabd3440, 2021.

999 Jahn, L. G., Jahl, L. G., Bland, G. D., Bowers, B. B., Monroe, L. W., and Sullivan, R. C.:
1000 Metallic and crustal elements in biomass-burning aerosol and ash: Prevalence, significance, and
1001 similarity to soil particles, *ACS Earth Space Chem.*, 5, 136-148, 2020.

1002 Jain, P., Sharma, A. R., Acuna, D. C., Abatzoglou, J. T., and Flannigan, M.: Record-breaking fire
1003 weather in North America in 2021 was initiated by the Pacific northwest heat dome, *Commun.*
1004 *Earth Environ.*, 5, 202, 2024.

1005 Kanji, Z. A., Ladino, L. A., Wex, H., Boose, Y., Burkert-Kohn, M., Cziczo, D. J., and Krämer,
1006 M.: Overview of Ice Nucleating Particles, Meteor. Monogr., 58, 1.1-1.33,
1007 <https://doi.org/10.1175/amsmonographs-d-16-0006.1>, 2017.

1008 Kiselev, A., Bachmann, F., Pedevilla, P., Cox, S. J., Michaelides, A., Gerthsen, D., and Leisner,
1009 T.: Active sites in heterogeneous ice nucleation—the example of K-rich feldspars, Science, 355,
1010 367-371, <https://doi.org/10.1126/science.aai8034>, 2017.

1011 Knippertz, P. and Stuut, J.-B. W.: Mineral dust, Mineral dust—A key player in the Earth system,
1012 121-147, Springer, 2014.

1013 Kobziar, L. N., Lampman, P., Tohidi, A., Kochanski, A. K., Cervantes, A., Hudak, A. T.,
1014 McCarley, R., Gullett, B., Aurell, J., and Moore, R.: Bacterial emission factors: a foundation for
1015 the terrestrial-atmospheric modeling of bacteria aerosolized by wildland fires, Environ. Sci.
1016 Technol., 58, 2413-2422, 2024.

1017 Koehler, K. A., Kreidenweis, S. M., DeMott, P. J., Prenni, A. J., and Petters, M. D.: Potential
1018 impact of Owens (dry) Lake dust on warm and cold cloud formation, J. Geophys. Res: Atmos.,
1019 112, 2007.

1020 Kotchenruther, R. A.: Source apportionment of PM_{2.5} at IMPROVE monitoring sites within and
1021 outside of marine vessel fuel sulfur emissions control areas, J Air Waste Manag Assoc, 71, 1114-
1022 1126, <https://doi.org/10.1080/10962247.2021.1917463>, 2021.

1023 Kuang, C., Singh, A., Howie, J., Salwen, C., & Hayes, C. Scanning mobility particle sizer
1024 (AOSSMPS), 2021-10-27 to 2023-06-16, ARM Mobile Facility (GUC), Gunnison, CO;
1025 Supplemental Facility 2 (S2). Atmospheric Radiation Measurement (ARM) User Facility.
1026 <https://doi.org/10.5439/1476898>, Data accessed 2024-08-01.

1027 Lacher, L., Steinbacher, M., Bukowiecki, N., Herrmann, E., Zipori, A., and Kanji, Z. A.: Impact
1028 of Air Mass Conditions and Aerosol Properties on Ice Nucleating Particle Concentrations at the
1029 High Altitude Research Station Jungfraujoch, Atmosphere, 9,
1030 <https://doi.org/10.3390/atmos9090363>, 2018.

1031 Liu, W. and Hopke, P. K.: Origins of fine aerosol mass in the western United States using positive
1032 matrix factorization, J. Geophys. Res: Atmos., 108, <https://doi.org/10.1029/2003jd003678>, 2003.

1033 Lohmann, U. and Feichter, J.: Global indirect aerosol effects: a review, Atmos. Chem. Phys., 5,
1034 715-737, <https://doi.org/10.5194/acp-5-715-2005>, 2005.

1035 Lynn, B., Khain, A., Rosenfeld, D., and Woodley, W. L.: Effects of aerosols on precipitation from
1036 orographic clouds, J. Geophys. Res: Atmos., 112, 2007.

1037 Malm, W. C., Sisler, J. F., Huffman, D., Eldred, R. A., and Cahill, T. A.: Spatial and seasonal
1038 trends in particle concentration and optical extinction in the United States, J. Geophys. Res:
1039 Atmos., 99, 1347-1370, 1994.

1040 Marinescu, P. J., Levin, E. J., Collins, D., Kreidenweis, S. M., and van den Heever, S. C.:
1041 Quantifying aerosol size distributions and their temporal variability in the Southern Great Plains,
1042 USA, Atmos. Chem. Phys., 19, 11985-12006, 2019.

1043 McCluskey, C. S., DeMott, P. J., Prenni, A. J., Levin, E. J. T., McMeeking, G. R., Sullivan, A. P.,
1044 Hill, T. C. J., Nakao, S., Carrico, C. M., and Kreidenweis, S. M.: Characteristics of atmospheric
1045 ice nucleating particles associated with biomass burning in the US: Prescribed burns and

1046 wildfires, *J. Geophys. Res: Atmos.*, 119, 10458-10470, <https://doi.org/10.1002/2014jd021980>,
1047 2014.

1048 McCluskey, C. S., Ovadnevaite, J., Rinaldi, M., Atkinson, J., Belosi, F., Ceburnis, D., Marullo,
1049 S., Hill, T. C. J., Lohmann, U., Kanji, Z. A., O'Dowd, C., Kreidenweis, S. M., and DeMott, P. J.:
1050 Marine and Terrestrial Organic Ice-Nucleating Particles in Pristine Marine to Continentally
1051 Influenced Northeast Atlantic Air Masses, *J. Geophys. Res: Atmos.*, 123, 6196-6212,
1052 <https://doi.org/10.1029/2017jd028033>, 2018a.

1053 McCluskey, C. S., Hill, T. C. J., Malfatti, F., Sultana, C. M., Lee, C., Santander, M. V., Beall, C.
1054 M., Moore, K. A., Cornwell, G. C., Collins, D. B., Prather, K. A., Jayarathne, T., Stone, E. A.,
1055 Azam, F., Kreidenweis, S. M., and DeMott, P. J.: A Dynamic Link between Ice Nucleating
1056 Particles Released in Nascent Sea Spray Aerosol and Oceanic Biological Activity during Two
1057 Mesocosm Experiments, *J. Atmos. Sci.*, 74, 151-166, <https://doi.org/10.1175/Jas-D-16-0087.1>,
1058 2017.

1059 McCluskey, C. S., Hill, T. C. J., Humphries, R. S., Rauker, A. M., Moreau, S., Strutton, P. G.,
1060 Chambers, S. D., Williams, A. G., McRobert, I., Ward, J., Keywood, M. D., Harnwell, J.,
1061 Ponsonby, W., Loh, Z. M., Krummel, P. B., Protat, A., Kreidenweis, S. M., and DeMott, P. J.:
1062 Observations of Ice Nucleating Particles Over Southern Ocean Waters, *Geophys. Res. Lett.*, 45,
1063 <https://doi.org/10.1029/2018gl079981>, 2018b.

1064 Meng, X., Yu, Y., and Ginoux, P.: Rise in dust emissions from burned landscapes primarily
1065 driven by small fires, *Nat. Geosci.*, 18, 586-592, <https://doi.org/10.1038/s41561-025-01730-3>,
1066 2025.

1067 Meyers, M. P., DeMott, P. J., and Cotton, W. R.: New primary ice-nucleation parameterizations
1068 in an explicit cloud model, *J. Appl. Meteor. Climatol.*, 31, 708-721, 1992.

1069 Miltenberger, A. K., Field, P. R., Hill, A. A., Rosenberg, P., Shipway, B. J., Wilkinson, J. M.,
1070 Scovell, R., and Blyth, A. M.: Aerosol–cloud interactions in mixed-phase convective clouds–Part
1071 1: Aerosol perturbations, *Atmos. Chem. Phys.*, 18, 3119-3145, 2018.

1072 Mignani, C., Hill, T. C. J., Nieto-Caballero, M., Barry, K. R., Bryan, N. C., Marinescu, P. J.,
1073 Dolan, B., Sullivan, A. P., Hernandez, M., Bosco-Lauth, A., van den Heever, S. C., Stone, E. A.,
1074 Grant, L. D., Perkins, R. J., DeMott, P. J., and Kreidenweis, S. M.: Ice-Nucleating Particles Are
1075 Emitted by Raindrop Impact, *J. Geophys. Res: Atmos.*, 130,
1076 <https://doi.org/10.1029/2024jd042584>, 2025.

1077 Murray, B. J., O'Sullivan, D., Atkinson, J. D., and Webb, M. E.: Ice nucleation by particles
1078 immersed in supercooled cloud droplets, *Chem Soc Rev*, 41, 6519-6554,
1079 <https://doi.org/10.1039/c2cs35200a>, 2012.

1080 Niemand, M., Möhler, O., Vogel, B., Vogel, H., Hoose, C., Connolly, P., Klein, H., Bingemer, H.,
1081 DeMott, P., Skrotzki, J., and Leisner, T.: A Particle-Surface-Area-Based Parameterization of
1082 Immersion Freezing on Desert Dust Particles, *J. Atmos. Sci.*, 69, 3077-3092,
1083 <https://doi.org/10.1175/Jas-D-11-0249.1>, 2012.

1084 Norris, G., Duvall, R., Brown, S., and Bai, S.: EPA positive matrix factorization (PMF) 5.0
1085 fundamentals and user guide, US Environmental Protection Agency, Washington, DC, www2.epa.gov/sites/production/files/2015-02/documents/pmf_5.0_user_guide.pdf, 2014.

1087 O'Sullivan, D., Murray, B. J., Ross, J. F., and Webb, M. E.: The adsorption of fungal ice-
1088 nucleating proteins on mineral dusts: a terrestrial reservoir of atmospheric ice-nucleating
1089 particles, *Atmos. Chem. Phys.*, 16, 7879-7887, <https://doi.org/10.5194/acp-16-7879-2016>, 2016.

1090 O'Sullivan, D., Murray, B. J., Malkin, T. L., Whale, T. F., Umo, N. S., Atkinson, J. D., Price, H.
1091 C., Baustian, K. J., Browse, J., and Webb, M. E.: Ice nucleation by fertile soil dusts: relative
1092 importance of mineral and biogenic components, *Atmos. Chem. Phys.*, 14, 1853-1867,
1093 <https://doi.org/10.5194/acp-14-1853-2014>, 2014.

1094 Pereira, D. L., Gavilán, I., Letechipía, C., Raga, G. B., Puig, T. P., Mugica-Álvarez, V., Alvarez-
1095 Ospina, H., Rosas, I., Martínez, L., Salinas, E., Quintana, E. T., Rosas, D., and Ladino, L. A.:
1096 Mexican agricultural soil dust as a source of ice nucleating particles, *Atmos. Chem. Phys.*, 22,
1097 6435-6447, <https://doi.org/10.5194/acp-22-6435-2022>, 2022.

1098 Pratt, K. A., DeMott, P. J., French, J. R., Wang, Z., Westphal, D. L., Heymsfield, A. J., Twohy, C.
1099 H., Prenni, A. J., and Prather, K. A.: In situ detection of biological particles in cloud ice-crystals,
1100 *Nat. Geosci.*, 2, 398-401, <https://doi.org/10.1038/ngeo521>, 2009.

1101 Pratt, K. A., Twohy, C. H., Murphy, S. M., Moffet, R. C., Heymsfield, A. J., Gaston, C. J.,
1102 DeMott, P. J., Field, P. R., Henn, T. R., Rogers, D. C., Gilles, M. K., Seinfeld, J. H., and Prather,
1103 K. A.: Observation of playa salts as nuclei in orographic wave clouds, *J. Geophys. Res: Atmos.*,
1104 115, <https://doi.org/10.1029/2009jd013606>, 2010.

1105 Prenni, A. J., DeMott, P. J., Sullivan, A. P., Sullivan, R. C., Kreidenweis, S. M., and Rogers, D.
1106 C.: Biomass burning as a potential source for atmospheric ice nuclei: Western wildfires and
1107 prescribed burns, *Geophys. Res. Lett.*, 39, <https://doi.org/10.1029/2012gl051915>, 2012.

1108 Prenni, A. J., Tobo, Y., Garcia, E., DeMott, P. J., Huffman, J. A., McCluskey, C. S., Kreidenweis,
1109 S. M., Prenni, J. E., Pöhlker, C., and Pöschl, U.: The impact of rain on ice nuclei populations at a
1110 forested site in Colorado, *Geophys. Res. Lett.*, 40, 227-231,
1111 <https://doi.org/10.1029/2012gl053953>, 2013.

1112 Reicher, N., Budke, C., Eickhoff, L., Raveh-Rubin, S., Kaplan-Ashiri, I., Koop, T., and Rudich,
1113 Y.: Size-dependent ice nucleation by airborne particles during dust events in the eastern
1114 Mediterranean, *Atmos. Chem. Phys.*, 19, 11143-11158, 2019.

1115 Rolph, G., Stein, A., and Stunder, B.: Real-time environmental applications and display system:
1116 *READY*, *Environ. Model. Softw.*, 95, 210-228, 2017.

1117 Sanchez-Marroquin, A., West, J. S., Burke, I. T., McQuaid, J. B., and Murray, B. J.: Mineral and
1118 biological ice-nucleating particles above the South East of the British Isles, *Environ. Sci. Atmos.*,
1119 1, 176-191, <https://doi.org/10.1039/d1ea00003a>, 2021.

1120 Schill, G. P., DeMott, P. J., Emerson, E. W., Rauker, A. M. C., Kodros, J. K., Suski, K. J., Hill, T.
1121 C. J., Levin, E. J. T., Pierce, J. R., Farmer, D. K., and Kreidenweis, S. M.: The contribution of
1122 black carbon to global ice nucleating particle concentrations relevant to mixed-phase clouds,
1123 *Proc. Natl. Acad. Sci. USA*, 117, 22705-22711, <https://doi.org/10.1073/pnas.2001674117>, 2020.

1124 Schnell, R. C. and Vali, G.: Looking Back: An Account of How Ice Nucleation by Bacteria Was
1125 Discovered (1963 to about Mid-1980s). Part II: Broadening the Scope, *Bull. Amer. Meteor. Soc.*,
1126 105, E1004-E1014, <https://doi.org/10.1175/bams-d-23-0115.1>, 2024.

1127 Seinfeld, J. H. and Pandis, S. N.: Atmospheric chemistry and physics: from air pollution to
1128 climate change, 3rd edn., Wiley, Hoboken, NJ, 2016.

1129 Seinfeld, J. H., Bretherton, C., Carslaw, K. S., Coe, H., DeMott, P. J., Dunlea, E. J., Feingold, G.,
1130 Ghan, S., Guenther, A. B., Kahn, R., Kraucunas, I., Kreidenweis, S. M., Molina, M. J., Nenes,
1131 A., Penner, J. E., Prather, K. A., Ramanathan, V., Ramaswamy, V., Rasch, P. J., Ravishankara, A.
1132 R., Rosenfeld, D., Stephens, G., and Wood, R.: Improving our fundamental understanding of the
1133 role of aerosol-cloud interactions in the climate system, Proc. Natl. Acad. Sci. USA, 113, 5781-
1134 5790, <https://doi.org/10.1073/pnas.1514043113>, 2016.

1135 Shawon, A. S. M., Benedict, K. B., Gutierrez, A., and Aiken, A. C.: Diurnal Trends and
1136 Meteorological Factors Influencing the Variability of Fluorescent Bioaerosol in Mt. Crested
1137 Butte, Colorado During SAIL, J. Geophys. Res: Atmos., 130,
1138 <https://doi.org/10.1029/2024jd041186>, 2025.

1139 Shi, Y., Creamean, J., Hill, T., Hume, C., & Vazquez, M. Ice Nucleation Spectrometer for INP
1140 measurement (INP), 2021-09-09 to 2023-06-12, ARM Mobile Facility (GUC), Gunnison, CO;
1141 Supplemental Facility 2 (S2). Atmospheric Radiation Measurement (ARM) User Facility.
1142 <https://doi.org/10.5439/1770816>, Data accessed 2025-05-01.

1143 Shi, Y. and Liu, X.: Dust radiative effects on climate by glaciating mixed-phase clouds, Geophys.
1144 Res. Lett., 46, 6128-6137, 2019.

1145 Stein, A. F., Draxler, R. R., Rolph, G. D., Stunder, B. J., Cohen, M. D., and Ngan, F.: NOAA's
1146 HYSPLIT atmospheric transport and dispersion modeling system, Bull. Amer. Meteor. Soc., 96,
1147 2059-2077, 2015.

1148 Steinke, I., Funk, R., Busse, J., Iturri, A., Kirchen, S., Leue, M., Möhler, O., Schwartz, T.,
1149 Schnaiter, M., Sierau, B., Toprak, E., Ullrich, R., Ulrich, A., Hoose, C., and Leisner, T.: Ice
1150 nucleation activity of agricultural soil dust aerosols from Mongolia, Argentina, and Germany, J.
1151 Geophys. Res: Atmos., 121, <https://doi.org/10.1002/2016jd025160>, 2016.

1152 Storelvmo, T., Hoose, C., and Eriksson, P.: Global modeling of mixed-phase clouds: The albedo
1153 and lifetime effects of aerosols, J. Geophys. Res: Atmos., 116, 2011.

1154 Sun, Y., Zhu, Y., Qi, Y., Chen, L., Mu, J., Shan, Y., Yang, Y., Nie, Y., Liu, P., Cui, C., Zhang, J.,
1155 Liu, M., Zhang, L., Wang, Y., Wang, X., Tang, M., Wang, W., and Xue, L.: Measurement report:
1156 Atmospheric ice nuclei in the Changbai Mountains (2623 m a.s.l.) in northeastern Asia, Atmos.
1157 Chem. Phys., 24, 3241-3256, <https://doi.org/10.5194/acp-24-3241-2024>, 2024.

1158 Suski, K. J., Hill, T. C., Levin, E. J., Miller, A., DeMott, P. J., and Kreidenweis, S. M.:
1159 Agricultural harvesting emissions of ice-nucleating particles, Atmos. Chem. Phys., 18, 13755-
1160 13771, 2018.

1161 Testa, B., Hill, T. C. J., Marsden, N. A., Barry, K. R., Hume, C. C., Bian, Q., Uetake, J., Hare, H.,
1162 Perkins, R. J., Möhler, O., Kreidenweis, S. M., and DeMott, P. J.: Ice Nucleating Particle
1163 Connections to Regional Argentinian Land Surface Emissions and Weather During the Cloud,
1164 Aerosol, and Complex Terrain Interactions Experiment, J. Geophys. Res: Atmos., 126,
1165 <https://doi.org/10.1029/2021jd035186>, 2021.

1166 Tobo, Y., DeMott, P. J., Hill, T. C. J., Prenni, A. J., Swoboda-Colberg, N. G., Franc, G. D., and
1167 Kreidenweis, S. M.: Organic matter matters for ice nuclei of agricultural soil origin, Atmos.
1168 Chem. Phys., 14, 8521-8531, <https://doi.org/10.5194/acp-14-8521-2014>, 2014.

1169 Tobo, Y., Prelli, A. J., DeMott, P. J., Huffman, J. A., McCluskey, C. S., Tian, G., Pöhlker, C.,
1170 Pöschl, U., and Kreidenweis, S. M.: Biological aerosol particles as a key determinant of ice
1171 nuclei populations in a forest ecosystem, *J. Geophys. Res: Atmos.*, 118,
1172 <https://doi.org/10.1002/jgrd.50801>, 2013.

1173 Umo, N. S., Murray, B. J., Baeza-Romero, M. T., Jones, J. M., Lea-Langton, A. R., Malkin, T. L.,
1174 O'Sullivan, D., Neve, L., Plane, J. M. C., and Williams, A.: Ice nucleation by combustion ash
1175 particles at conditions relevant to mixed-phase clouds, *Atmos. Chem. Phys.*, 15, 5195-5210,
1176 <https://doi.org/10.5194/acp-15-5195-2015>, 2015.

1177 Vali, G.: Quantitative evaluation of experimental results on the heterogeneous freezing
1178 nucleation of supercooled liquids, *J. Atmos. Sci.*, 28, 402-409, 1971.

1179 Vali, G. and Schnell, R. C.: Looking Back: An Account of How Ice Nucleation by Bacteria Was
1180 Discovered (1963 to about Mid-1980s). Part I: The Basics, *Bull. Amer. Meteor. Soc.*, 105, E778-
1181 E788, <https://doi.org/10.1175/bams-d-23-0114.1>, 2024.

1182 Vivioli, D., Dürr, H. H., Messerli, B., Meybeck, M., and Weingartner, R.: Mountains of the
1183 world, water towers for humanity: Typology, mapping, and global significance, *Water Resour.*
1184 *Res.*, 43, 2007.

1185 Wagner, R., Jähn, M., and Schepanski, K.: Wildfires as a source of airborne mineral dust—
1186 revisiting a conceptual model using large-eddy simulation (LES), *Atmos. Chem. Phys.*, 18,
1187 11863-11884, 2018.

1188 Wilson, T. W., Ladino, L. A., Alpert, P. A., Breckels, M. N., Brooks, I. M., Browne, J., Burrows,
1189 Carslaw, K. S., Huffman, J. A., Judd, C., Kilthau, W. P., Mason, R. H., McFiggans, G.,
1190 Miller, L. A., Najera, J. J., Polishchuk, E., Rae, S., Schiller, C. L., Si, M., Temprado, J. V., Whale,
1191 T. F., Wong, J. P., Wurl, O., Yakobi-Hancock, J. D., Abbatt, J. P., Aller, J. Y., Bertram, A. K.,
1192 Knopf, D. A., and Murray, B. J.: A marine biogenic source of atmospheric ice-nucleating
1193 particles, *Nature*, 525, 234-238, <https://doi.org/10.1038/nature14986>, 2015.

1194 Zhao, X., Jiang, K., Ou'yang, S., Li, Y., Wang, Y., Wang, J., Zhao, N., and Shen, G.: Global
1195 Biomass Burning Emission Contributions to Ice Nucleating Particles, *Geophys. Res. Lett.*, 51,
1196 <https://doi.org/10.1029/2024gl111881>, 2024.

1197 Ruichen Zhou, Russell Perkins, Sonia Kreidenweis. Source apportionment of aerosols at the White
1198 River IMPROVE site near the SAIL site. ARM Data Collection, Oak Ridge National Laboratory,
1199 U.S. Department of Energy, Oak Ridge, Tennessee, USA. Dataset accessed on 2025.
1200 <https://doi.org/10.5439/2573028>, 2025a.

1201 Ruichen Zhou, Russell Perkins, Sonia Kreidenweis, Kelton Ayars. Back trajectories during SAIL.
1202 ARM Data Collection, Oak Ridge National Laboratory, U.S. Department of Energy, Oak Ridge,
1203 Tennessee, USA. Dataset accessed on 2025. <https://doi.org/10.5439/2574969>, 2025a.

1204 Ruichen Zhou, Russell Perkins, Sonia Kreidenweis. Merged aerosol size distribution from SMPS
1205 and OPC for SAIL. ARM Data Collection, Oak Ridge National Laboratory, U.S. Department of
1206 Energy, Oak Ridge, Tennessee, USA. Dataset accessed on 2025.
1207 <https://doi.org/10.5439/2572899>, 2025a.

1208